

POLITECNICO DI MILANO

Faculty of Industrial Engineering

Master of Science in Mechanical Engineering



Mechanical design of an IR camera optical bench for Juno Mission

Advisor: Prof. Bortolino SAGGIN

Co-advisor: Ing. Marco TARABINI

Master Thesis of:

Davide MAURI Matr. 740210

Academic Year 2009 - 2010

Acknowledgements

Questa tesi la dedico a tutti coloro che mi hanno permesso di arrivare a questo importante traguardo.

Il primo ringraziamento va alla mia famiglia che, in tutti questi anni, con enormi sacrifici è riuscita a supportare i miei studi e le mie necessità. A mia sorella e a Fabio va il mio grazie per essere, la prima, il miglior medico che si possa avere e il secondo per essere un ottimo cognato.

Un grazie speciale a *Flavia* che, con amore e dolcezza, mi è stata vicina in questi anni di studio. Con lei, ho affrontato i momenti belli e le difficoltà della vita, sempre sicuro di avere una persona speciale al mio fianco.

Un grazie a tutti i miei *Amici e compagni di università* con i quali ho condiviso le mie lunghe giornate di studio, gli esami e tutti quei momenti indimenticabili di vera amicizia.

Ed infine un grazie a tutte quelle persone che ho avuto il piacere di incontrare nella vita che, per un motivo o per l'altro, hanno creduto in me.

A tutti questi un grazie di cuore.

Davide

Contents

Chapter 1	The JGO Mission	17
1.1.	Jupiter Ganymede Orbiter's Mission.....	17
1.1.1.	Mission details	19
1.1.2.	Jupiter	20
1.1.3.	Jupiter's Moons	22
1.1.4.	Magnetosphere	23
1.1.5.	Magnetosphere measurements	23
1.1.6.	Atmosphere observations	24
1.1.7.	Callisto Observations	24
1.1.8.	Ganymede Observations	24
1.2.	Instrument description	25
1.2.1.	Design requirements.....	26
1.2.2.	Scope of the thesis.....	26
1.2.3.	Materials properties.....	27
1.3.	Finite elements analysis (FEM).....	29
1.3.1.	Fem history.....	29
1.3.2.	Characteristics and problems related to FEM	30
Chapter 2	Instrument model design	31
2.1.	Introduction	31
2.2.	Geometrical parameters definition	31
2.3.	FEM analysis' parameters	36
2.4.	Models design.....	37
2.4.1.	Single smooth plane model	37
2.4.2.	Double smooth plane model.....	39
2.4.3.	Single plane model with ribs.....	40

2.4.4.	Double plane model with ribs.....	41
2.4.5.	Consideration about results.....	42
Chapter 3	Optics supports design.....	43
3.1.	Introduction.....	43
3.2.	Lens 1: support model design	44
3.2.1.	First lens support configurations	44
3.2.2.	Lens 1: definitive support model	46
3.2.3.	Natural frequencies analysis	47
3.2.4.	Static analysis	48
3.3.	Lens 2: support model design	52
3.4.	Lens 3: support model design	56
3.4.1.	Natural frequencies analysis	57
3.4.2.	Static analysis	58
3.5.	Lens 4: support model design	60
3.5.1.	Natural frequencies analysis	60
3.5.2.	Natural frequencies consideration	61
3.5.3.	Static analysis	62
3.6.	Alternative solution for lenses 3 and 4 supports	65
3.7.	Lens 5: support model design	67
3.8.	Screws design.....	67
3.8.1.	Screw design for other parts	69
Chapter 4	Optical bench design optimization	71
4.1.	Introduction.....	71
4.2.	Optical bench ribs optimization	71
4.2.1.	General plane dimensions definition	71
4.2.2.	Ribbed plane design.....	72
Chapter 5	Optical Bench Supports	77
5.1.	Introduction.....	77

5.2.	Geometry of the supports definition.....	79
5.3.	Peak load analysis.....	79
5.3.1.	Eulero theory	79
5.3.2.	Peak analysis applied to supports.....	82
5.4.	Thermal analysis of supports.....	85
5.4.1.	Thermal analysis theory	85
5.4.2.	Thermal analysis applied to supports	85
5.5.	Peak load and thermal analysis comparison.....	86
Chapter 6	Final Model Design.....	89
6.1.	Definitive ribbed instrument base	89
6.2.	Total model analysis.....	91
Chapter 7	TM Covering systems	95
7.1.1.	Covering system model.....	95
7.1.2.	Frequency analysis on TM's cover system	97
7.1.3.	Static analysis with imposed acceleration on TM's cover system	99
7.2.	Thermal Mapper covering system conclusion.....	99
Chapter 8	Conclusions	101
Chapter 9	References	105
Chapter 10	Appendix	107

Figures and Tables List

Figure 1.1 <i>Solar system</i>	17
Figure 1.2 <i>Arianne V</i>	18
Figure 1.3 <i>Jupiter</i>	20
Figure 1.4 <i>Jupiter Moons</i>	22
Table 1.2 <i>Galilean moons parameters</i>	22
Figure 1.5 <i>Aurora borealis on Jupiter. Three bright dots are created by magnetic flux tubes that connect to the Jovian moons Io (on the left), Ganymede (on the bottom) and Europa (also on the bottom).</i>	23
Table 1.3 <i>Material properties</i>	28
Figure 2.1. <i>Lenses system and beam path of the first JGO model</i>	32
Figure 2.2 <i>Minimum dimension for the base. The red line represents the outgoing IR beam.</i>	33
Figure 2.3 <i>Lens support type 1</i>	34
Figure 2.4 <i>Lens support type 2</i>	34
Figure 2.5 <i>Instrument support</i>	35
Figure 2.6 <i>Ground constraint applied to instrument support</i>	36
Figure 2.7 <i>Simple blocked element constraint</i>	36
Figure 2.8 <i>Single plane model</i>	38
Table 2.1 <i>Weight and natural frequencies associated to the single plane model. Only the first three vibration modes results are here reported.</i>	38
Figure 2.9 <i>Two plane model</i>	39
Table 2.2 <i>Weight and natural frequencies associated to the double plane model. Only the first three vibration modes results are here reported.</i>	39
Figure 2.10 <i>Single plane model with ribs (bottom view)</i>	40
Figure 2.11 <i>Axonometric view of hide ribs pattern in single plane model</i>	40
Figure 2.12 <i>Double plane model with ribs</i>	41

Table 2.4. <i>Weight and natural frequencies associated to the double plane model with ribs. Only the first three vibration modes results are here reported.</i>	42
Figure 3.1 <i>Lenses nomenclature</i>	43
Figure 3.2 <i>Lens number 1 support. First model</i>	44
Figure 3.4 <i>Lens number 1 support model.</i>	46
Figure 3.5 <i>Natural frequencies analysis.</i>	47
Table 3.1 <i>Natural frequencies</i>	47
Figure 3.6 <i>Acceleration along z-axis</i>	48
Figure 3.7 <i>Acceleration along x-axis</i>	48
Figure 3.8 <i>Acceleration along y-axis</i>	49
Figure 3.9 <i>Static FEM Analysis. 600m/s² along z-axis direction</i>	49
Figure 3.10 <i>Acceleration acting along y-axis</i>	50
Figure 3.11 <i>Static FEM Analysis. 600m/s² along x-axis direction</i>	51
Figure 3.12 <i>Lens 2 support model.</i>	52
Figure 3.13 <i>Lens 2 support frequency analysis.</i>	52
Table 3.2 <i>Natural frequencies</i>	53
Figure 3.14 <i>Static analysis with 600m/s² applied along z-axis.</i>	53
Figure 3.15 <i>Static analysis with 600m/s² applied along x-axis.</i>	54
Figure 3.16 <i>Lens number 3 support.</i>	56
Figure 3.17 <i>Lens 3 support base pins.</i>	56
Figure 3.18 <i>Lens 3 support under FEM investigation.</i>	57
Table 3.3 <i>Natural frequencies</i>	57
Figure 3.19 <i>Acceleration applied along z-axis direction</i>	58
Figure 3.20 <i>Acceleration acting along x-axis.</i>	59
Figure 3.21 <i>Acceleration acting along y-axis</i>	59
Figure 3.22 <i>Lens 4 support model.</i>	60
Figure 3.23 <i>Lens 4 support model.</i>	60
Table 3.4 <i>Natural frequencies</i>	61
Figure 3.24 <i>Static analysis with 600m/s² applied along z-axis.</i>	62

Figure 3.25 Static analysis with $600m/s^2$ applied along x-axis.	62
Figure 3.26 Acceleration acting along y-axis	63
Figure 3.27 Modified model for lens 3 support	65
Figure 3.28 Static analysis on modified lens 3 support	66
Table 3.5 UNI 4535	68
Table 3.6 Characteristics of the screw UNI 5931 - M3	69
Figure 3.29 Screw.....	69
Figure 4.1 Definitive dimension for instrument base	72
Table 4.1. Ribs pattern analysis	73
Table 4.2 Quasi definitive model	75
Figure 5.1 JGO Instrument base support	77
Figure 5.2 First rough situation for JGO Instrument base support	78
Figure 5.3 a) Squat bar. b) Long length bar	79
Figure 5.4 Value of l_0 with its dependency on constraints types	80
Figure 5.5 External load applied to the instrument support	82
5.1. Peak load and Thermal Analysis comparison ($WT=0.15mm$)	86
Figure 5.6. Instrument support dimensions	87
Figure 6.1. Instrument base support	89
Figure 6.2. Instrument base support perspective	90
Figure 6.3. Complete model	90
Figure 6.4 2D draw of Instrument base	91
Figure 6.5 Definitive model frequency analysis	92
Figure 6.6 First vibration mode	92
Figure 6.7 Acceleration acting along z-axis	93
Figure 6.8 Total model analysis with acceleration acting on x-axis.....	94
Table 6.1 Principal characteristics of total model.....	94
Figure 7.1 Coverign system.....	95
Figure 7.2 Top of the TM covering system. Principal dimensions.....	96

Figure 7.3 Axonometric view of Thermal Mapper Covering system	96
Figure 7.4 Frontal part of the thermal mapper cover system.....	97
Figure 7.5 FEM analysis at 183 Hz for the cover system.....	98
Figure 7.6 Lateral view of top box surface at 384 Hz	98
Figure 7.7 Static analysis with acceleration acting along z-axis	99

Sommario

Nato dalla collaborazione tra le due agenzie spaziali, statunitense (NASA) ed europea (ESA), il progetto EJSM, acronimo di Europa Jupiter System Mission, prevede l'uso di due sonde per l'esplorazione del sistema gioviano. In particolare all'Agenzia Spaziale Europea è stata affidata la costruzione dei moduli Jupiter Ganymede Orbiter (JGO) e Jupiter Europa Orbiter. L'inizio della missione è stato programmato per il 2020, anno in cui le sonde verranno messe in orbita dal razzo Ariane V.

Il presente lavoro di tesi descrive la progettazione meccanica del *Thermal Mapper (TM)* presente nel modulo JGO. Questo strumento, composto principalmente da una struttura su cui sono montate le ottiche con i relativi supporti, orientato opportunamente, rileverà le caratteristiche dell'atmosfera gioviana determinando, inoltre, le attività vulcaniche dei satelliti Io e Icy.

In considerazione dei vincoli imposti dalla missione in termini di *mass budget* (imposto ad un massimo di 5 Kg per il modello completo) e di frequenze proprie (imposte ad un valore superiore ai 140 Hz), il lavoro di tesi si è articolato in diverse fasi di progettazione.

Trattandosi di uno studio di fattibilità, nella prima fase di questo lavoro di tesi, si è individuato un modello di riferimento comparando diverse soluzioni tecniche tra le quali il singolo e il doppio piano di appoggio per i supporti delle ottiche. Le diverse soluzioni sono state analizzate avvalendosi dell'uso del simulatore agli elementi finiti, presente nel software CAD Catia, per ciascuna configurazione è stata svolta la progettazione strutturale considerando in particolare i requisiti inerenti la prima frequenza propria e in secondo luogo effettuando verifiche di resistenza.

Lo studio si è poi focalizzato sulla definizione e ottimizzazione della struttura di supporto e isolamento termico con la quale, il Thermal Mapper, verrà montato sul satellite. Questa, oltre ai normali requisiti di massa e di prima frequenza propria del sistema completo, deve minimizzare lo scambio termico conduttivo tra il satellite e lo strumento stesso che per ragioni di riduzione dei disturbi deve essere raffreddato. Per tale motivo, di carico di punta e di resistenza termica, sono state condotte in parallelo per la progettazione di queste parti.

E' stato così possibile ottenere il modello complessivo del Thermal Mapper che costituisce ora la configurazione di base per questo strumento. Il risultato

rilevante è che la soluzione ottenuta una porta ad una massa della struttura di circa 0.8 kg con una prima frequenza propria di circa 160 Hz, entrambe le caratteristiche soddisfano i requisiti di progetto e permettono di documentare la fattibilità dello strumento.

Abstract

Born from the collaboration between American and European space agencies, the EJSM project, acronym of Europa Jupiter System Mission, will employ two spacecraft for the Jupiter's system exploration. Especially ESA has the hard work to built two modules: Jupiter Ganymede Orbiter (JGO) and Jupiter Europa Orbiter (JEO). The mission beginning is scheduled for the 2020, year in which the two spacecraft, will be launched on space by means of Ariane V.

This thesis is focused on the mechanical design of the Thermal Mapper (TM) that will be on the JGO module. This instrument, composed mainly by a structure upon which are mounted optics with relative supports, conveniently oriented, will point out Jupiter's atmosphere characteristics determining, furthermore, the volcanic activities of Io and Icy satellites.

In consideration of the constraints imposed by the mission in terms of mass budget (maximum allowable weight of the total instrument equal to 5 kg) and of natural frequency (imposed at a value higher than 140 Hz), the thesis work is structured into many design steps.

Considering, that this was the instrument feasibility study, in the first work phase, various models have been implemented, adopting different technical solution; for instance, the single and the double plane as optical bench structures, for mounting the optics supports. These last ones, thanks to FEM simulator of CATIA, have been designed, to be compliant with the requirements on the lower eigenfrequency and strength constraints.

The study, afterwards, has been focused on the supporting structure, which will connect the Thermal Mapper to the satellite. This structure in addition to the usual requirements on mass and stiffness and strength has to guarantee a low heat exchange between the instrument and the satellite, being the former cooled to reduce the thermal noise. For these reasons, thermal resistance analysis and structural analysis have been conducted in parallel.

The final result is the definition of an instrument structural configuration that is compatible with design constraints and in particular having a structure mass of 0.8 kg, and a natural frequency at 160 Hz.

Chapter 1

The JGO Mission

1.1. Jupiter Ganymede Orbiter's Mission

Nowadays the Jupiter system represent a way to better understand giant planets systems in general, which are now know to be present not only in the solar system, but also around other near-by stars. By contemplating the Jupiter system, and unraveling the history of the evolution of that system from its formation to the possible emergence of habitats and life, we will also shed a new light on the potential for the emergence of life in our galatic neighbourhood and beyond, and possibly considerably extend the potential for the emergence of life in our Galaxy.

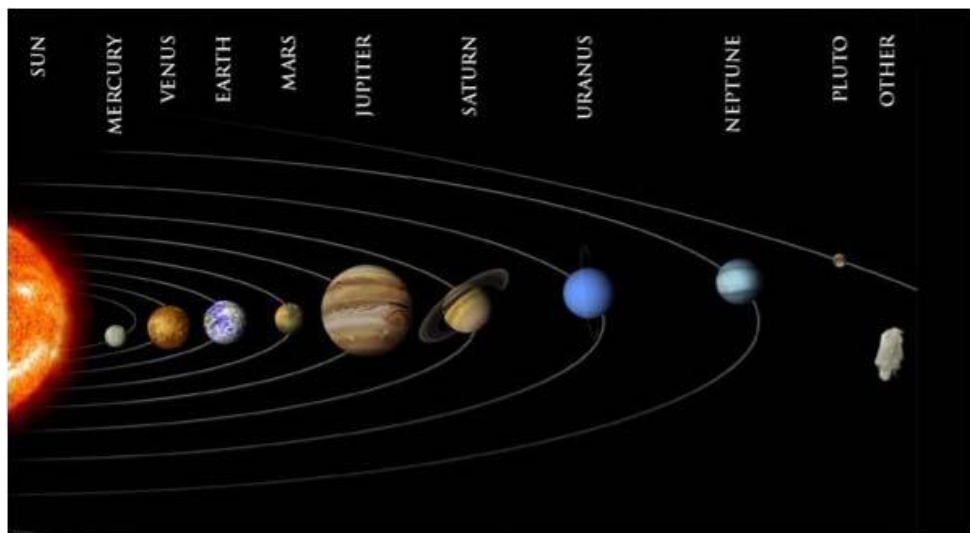


Figure 1.1 *Solar system*

Chapter 1

ESA's Cosmic Vision Laplace and NASA's mission to Europa joint into the international mission called "Europa Jupiter System Mission" (EJSM) [10]. The purpose is to study Jupiter and its magnetosphere, the diversity of the Galilean satellites, the physical characteristics, composition and geology of their surface, with a resolution higher than the one achieved by Galileo's mission.

The main objectives of the JGO (Jupiter Ganymede Orbiter) are: observation of Jupiter, its magnetosphere and the "icy" moons Ganymede and Callisto. In particular, in this mission it will determine the internal structure and the existence of subsurface oceans, the Laplace resonance and its role in maintaining tidal heating, an accurate analysis of satellites in infrared and in the visible fields.

The JGO mission is scheduled in 2020 from the launch pad of Kourou (French Guiana), by means of Ariane V ECA vehicle [1,9,10]. The geographic position of Kourou represent a perfect place to reach the geostationary transfer orbit since it lies at latitude $5^{\circ}3'$, just over 500 km north of the equator. This permits to take benefits from the so called 'slingshot' effect, that is the energy created by the speed of the Earth's rotation around the axis of the Poles. The main advantages of this effect is the increasing of the speed of the launchers by 460 m per second that, consequently, save fuel and money prolonging, at the same time, the active life of satellites.



Figure 1.2 *Ariane V*

The analysis of the preferred launch days points out that in March 11, 2020 is possible to reach a zero value for the escape declination, that represents the better situation for Ariane V [9]. Moreover, in the same days, it will be possible to reach a transfer time in the order of 5.9 years and a small DSM (Deep Space Manoeuvre).

After the escape from the Earth orbit, Ariane 5 will make the JGO able to follow a Venus-Earth-Earth route towards Jupiter after which, a complex sequence of swingbys with the Galilean moons will take place, and it will reach the orbit of Callisto with a low infinite velocity. Here the science is performed via a pseudo-orbiter technique. The spacecraft is then transferred to Ganymede where, after a capture into an elliptic orbit, the scanning of the moon's magnetosphere will occur followed by a circularization of the orbit in order to make a surface mapping.

1.1.1. Mission details

The entire mission can be divided into many steps:

1. Launch by Ariane 5 ECA into direct escape in March 2020;
2. Interplanetary VEEGA transfer with arrival at Jupiter in 2026;
3. Ganymede swingby and JOI puts the s/c into a highly elliptic orbit;
4. Series of ΔV gravity assist with Ganymede to reduce the apocenter and the inclination;
5. Transfer to Callisto and Pseudo-orbiter at Callisto;
6. Transfer to Ganymede with a Ganymede Orbit Insertion (GOI) into 200x6000 km elliptical orbit;
7. Science phase around Ganymede at low altitude (200 km) and with a circular, quasi-polar orbit;
8. End of nominal mission after about 8.9 years in February 2029;

And some rough mission's parameters can be pointed out as presented here:

1. Launch Mass Capability, 4362 kg
2. Launch Vehicle Adapter, 190 kg
3. Flight System Mass (CBE), 957 kg
4. Propellant (for 3000 m/s), 2562 kg
5. Remaining usable launch mass, 653 kg (for contingency and system margin)

1.1.2. Jupiter

Jupiter is the fifth planet from the Sun and the largest planet within the Solar System. It is a gas giant with a mass slightly less than one-thousandth of the Sun but is two and a half times the mass of all the other planets in our Solar System combined. Jupiter is classified as a gas giant along with Saturn, Uranus and Neptune. Together, these four planets are sometimes referred to as the Jovian planets.

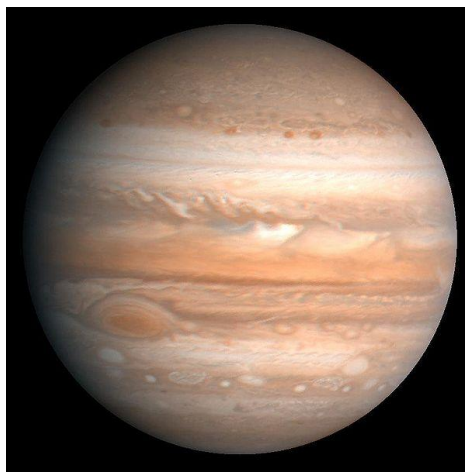


Figure 1.3 *Jupiter*

Jupiter is primarily composed of hydrogen with a quarter of its mass being helium; it may also have a rocky core of heavier elements. Because of its rapid rotation, Jupiter's shape is that of an oblate spheroid (it possesses a slight but noticeable bulge around the equator). The outer atmosphere is visibly segregated into several bands at different latitudes, resulting in turbulence and storms along their interacting boundaries.

The core of Jupiter is often described as rocky, but its detailed composition is unknown, as are the properties of materials at the temperatures and pressures of those depths. The core region is surrounded by dense metallic hydrogen, which extends outward to about 78 percent of the radius of the planet. Rain-like droplets of helium and neon precipitate downward through this layer, depleting the abundance of these elements in the upper atmosphere.

Above the layer of metallic hydrogen lies a transparent interior atmosphere of liquid hydrogen and gaseous hydrogen, with the gaseous portion extending downward from the cloud layer to a depth of about 1,000 km.

Table 1.1 *Jupiter physic characteristics*

Equatorial Radius	71,492±4 km
Polar Radius	66,854 ± 10 km
Volume	1.43128×10 ¹⁵ km ³
Mass	1.8986×10 ²⁷ kg
Surface temperature	165 K at 1 bar level 112 K at 0.1 bar level
Surface Pressure	20÷200 kPa
Composition	89.8±2.0% Hydrogen 10.2±2.0% Helium 0.3% Methane 0.026% Ammonia 0.003% Hydrogen deuteride 0.0006% Ethane 0.0004% Water

1.1.3. Jupiter's Moons

The orbits of Io, Europa, and Jupiter has 63 named natural satellites. Of these, 47 are less than 10 kilometres in diameter and have only been discovered since 1975. The four largest moons, known as the "Galilean moons", are Io, Europa, Ganymede and Callisto.

Ganymede, some of the largest satellites in the Solar System, form a pattern known as a Laplace resonance; for every four orbits that Io makes around Jupiter, Europa makes exactly two orbits and Ganymede makes exactly one. This resonance causes the gravitational effects of the three large moons to distort their orbits into elliptical shapes, since each moon receives an extra tug from its neighbors at the same point in every orbit it makes. The tidal force from Jupiter, on the other hand, works to circularize their orbits.

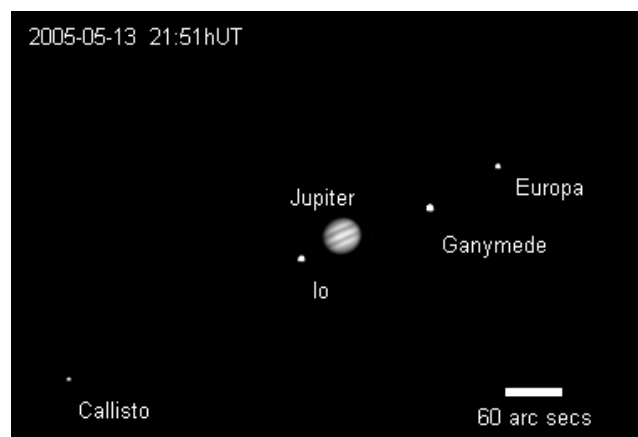


Figure 1.4 *Jupiter Moons*

Table 1.2 *Galilean moons parameters*

Name	Diameter	Mass	Orbital Radius	Orbital Period
	<i>km</i>	<i>kg</i>	<i>km</i>	<i>days</i>
Io	3643	8.9×10^{22}	421,700	1.77
Europa	3122	4.8×10^{22}	671,034	3.55
Ganymede	5262	14.8×10^{22}	1,070,412	7.15
Callisto	4821	10.8×10^{22}	1,882,709	16.69

1.1.4. Magnetosphere

Jupiter's broad magnetic field is 14 times as strong as the Earth's, ranging from 4.2 gauss (0.42 mT) at the equator to 10–14 gauss (1.0–1.4 mT) at the poles, making it the strongest in the Solar System. This field is believed to be generated by eddy currents — swirling movements of conducting materials— within the metallic hydrogen core. The field traps a sheet of ionized particles from the solar wind, generating a highly energetic magnetic field outside the planet: the magnetosphere. It is responsible for intense episodes of radio emission from the planet's polar regions. At about 75 Jupiter radii from the planet, the interaction of the magnetosphere with the solar wind generates a bow shock. The four largest moons of Jupiter all orbit within the magnetosphere, which protects them from the solar wind.

1.1.5. Magnetosphere measurements

Magnetospheric measurements [10] concern the characterisation of different neutral and charged particle populations, like electron and ion species, consistent of cold neutral and low-energy plasma; and hot neutral and high-energy charged particles including measurement of: density, velocity, pressure and their spatial and energy distribution functions.

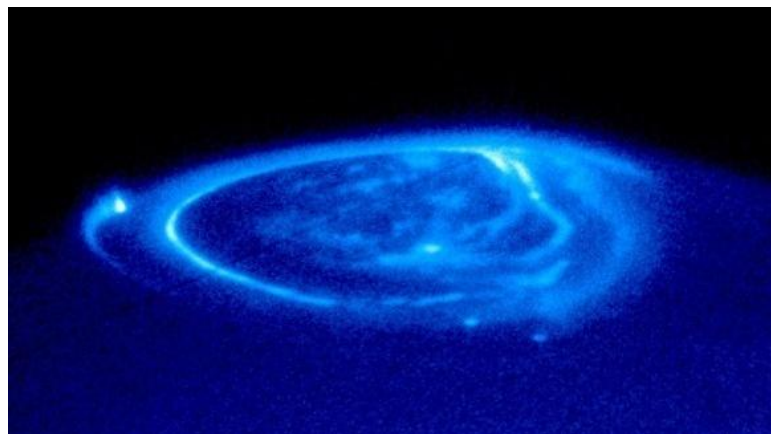


Figure 1.5 *Aurora borealis on Jupiter. Three bright dots are created by magnetic flux tubes that connect to the Jovian moons Io (on the left), Ganymede (on the bottom) and Europa (also on the bottom).*

Chapter 1

For this reason it will be present a plasma mass spectrometer able to conduct measurements at high value of energies (up to 100 keV/q), associated to a dedicated high energy instruments.

The characterization of electromagnetic field will be done by measuring the static magnetic field, the magnetic and electric components of high frequency fluctuations.

In addition dust parameters should be determined also with a chemical characterization.

1.1.6. Atmosphere observations

Observations of Jupiter atmosphere will require a repetition of measurements that will be done at short (hours), medium (a few Jovian days), long (weeks/months) and even very long time (years).

1.1.7. Callisto Observations

Callisto moon will be studied by a series of “fly-bys” that will address to the specific Callisto science objectives [10]. The main requirements for Callisto observations are: study the induced magnetic field, improve global coverage (imaging, and spectroscopy), topographic mapping of large fractions of the satellites’ surfaces, and many others.

1.1.8. Ganymede Observations

Ganymede is the largest satellite of the solar system and it is the main target of the JGO spacecraft [10]. The measurements will include the determination of the tidal response (amplitudes and phase lags) and a precise determination of the rotational state including physical librations. Topographic data will be additionally obtained to derive the exact shape of the satellite including the static and dynamic tidal response.

The location and extension of the ocean (located below a ~80 km thick ice shell) and its main characteristics, e.g., electrical conductivity, can be inferred by measuring Ganymede’s induced magnetic field using multiple frequencies. A profound determination of Ganymede’s intrinsic field is required

to disentangle the induced field (generated in the ocean) from the intrinsic field (generated in the iron core). The surface will be mapped using imaging data as well as spectroscopic measurements on global, regional, and local scales.

The following Ganymede orbit options shall be looked at:

Case 1: High-inclination circular orbit (200 km), which is preferred to achieve the geophysics/geochemistry/geology objectives;

Case 2: High-inclination elliptical orbit (nominal 200 km x 6000 km which may be allowed to drift), which is preferred for achieving the scientific objectives of Ganymede magnetospheric science;

Case 3: a combination of case 1 and case 2 shall be looked at

Case 4: a Pseudo-Orbit at Ganymede, which is a quasi-circular orbit around Jupiter that encounters regularly (every few days) Ganymede. Although it is understood that it may decrease Ganymede science capability, it may offer a larger payload capability. It may also offer the opportunity to go also in a pseudo-orbit at Callisto.

1.2. Instrument description

This thesis is concerned about the model definition for the Thermal Mapper (TM) that is composed by a structure upon which there are mounted some optics with respectively their supports. The characteristics of this Thermal Mapper is that it have to guarantee a natural frequency up to 140 Hz with a total mass lower than 5 Kg.

This TM will be mounted on the JGO satellite that will be in the space after the launch, by means of Ariane V, in 2020 and it will reach the Jupiter's Orbit after six years.

This instruments will be provided by some parts:

- *Optics (lenses):* instrument has four fixed optics, one moveable and tilt able by means of an electric motor;
- *Optics bench (Instrument base):* this could be made by ribbed or smooth plane and will provide the greatest contribution to the total stiffness of the instrument;

Chapter 1

- *Optics supports*: four supports guarantee the correct alignment of the lenses;
- *Electric motor*: A piezoelectric motor will tilt the principal lens with respect to the deep-space (this part is not subject of this thesis);
- *Instrument supports*: by means of four contact point with the satellite they give the link between the instrument base to the satellite itself giving, at the same time, an high thermal resistance with respect to the low mass budget and high required stiffness;

1.2.1. Design requirements

The main requirements for the design of the TM module are [8]:

1. The maximum value for total mass is 5 kg including shielding;
2. Total maximum power absorption is fixed at 5W;
3. Orbital circular speed around Ganymede at 200 km is equal to 1.5Km/sec;
4. The module must be smaller than the one used in THEMIS mission that was 25x25x30 cm;
5. It could be cooled;
6. It requires an absolute calibration;
7. The first natural frequency greater than 140 Hz;
8. Thermal stresses must be little theoretically null;

1.2.2. Scope of the thesis

This thesis is a preliminary study of all parts composing the Thermal Mapper since no previous model about it has been realized. The work can be summarized into many steps:

- *Definition of qualitative dimensions and geometry for the optics bench*: it will represent the greatest part of this thesis work. To achieve the minimum allowable dimensions for this part an accurate analysis of the optics disposition will be applied;
- *Definition of preliminary optics bench*: it involves the definition of a model for the optic bench in order to point out different solutions in

terms of geometry. Starting from one plane, configuration with multiple-plane will be take into account. Best solution will be chose according to the lower mass and higher natural frequency that will have a model with respect to others;

- *Optics supports definition:* single lens will be evaluated with respect to its geometry and mass; a support model will be defined in order to: guarantee its easily mounting on the bench ,to reach correct value of natural frequency and resistance at an imposed acceleration. Different models of supports will be pointed out;
- *First validation of optics bench:* according to the defined optics supports, the model of optics bench, will be validated by making new geometry and dimensions for its ribs pattern. Considering ideal constraints like clamps, that overestimate the frequency results, or hinges that underestimate the results, will be possible to achieve the first validated model for the optics bench;
- *Bench supports design:* in this phase will be studied the system that will permits to the optics bench to be mounted on the satellite. According to previous studies conducted on similar parts of another space mission will be take into account the tubular V-Shaped solution. Thermal analysis and peak load analysis will be evaluated in this thesis part;
- *Final validation of optics bench and total instrument assembling:* definitive configuration will be obtained assembling all modelled parts together; FEM analysis will confirm the last model as the optimal one by overcoming the threshold imposed to the natural frequency and respecting the mass budget;
- *Preliminary study of Thermal Mapper covering system:* will be modelled a conceptual cover for the instrument. Will be referred to previous study conducted on MIMA mission.

1.2.3. Materials properties

The choice of the material is one of the most design critical points that has a great influence on all the results. In particular, in aerospace engineering, it is usual to work at extreme conditions for what concern the saving of mass with having, at the same time, high mechanical properties and high value of stiffness. In this thesis there are two main constraints for the design: maximum mass allowed is fixed at 5 kg and natural frequency must be greater than 140 Hz.

Chapter 1

Since this thesis work starts without a pre-model (the only thing in our possession is the lenses system) the first step could be the choice of material, but, since no parts are already modeled this step goes as second point. In fact, at the begin, it has been choice to start adopting as material the CATIA's standard aluminium.

After a preliminary analysis of the models, in order to define some geometry and dimensions, it was possible to analyse the same configuration but taking into account other kind of materials.

Searching on web and looking to previous mission and literature, some material could be considered as standard for space missions. Between these we can find: carbon and glass fibre, Ergal, Kevlar, aluminium and titanium with, eventually, particular addition of some alloy elements. Some previous study advise carbon fibre as one of the best material since it has a great balance between stiffness, mass and thermal conductivity [4,5,6].

Table 1.3 *Material properties*

MATERIAL		ERGAL	TITANIUM	COMPOSITE FIBRE	CARBON FIBRE	Al-Be
Young Modulus	GPa	70	114	70	110	205
Density	kg/m ³	2800	4.4	1500	1700	2800
Poisson Coeff.		0.33	0.34	0.20	0.25	0.29
	MPa	570	800	400	-	-
Yield point	MPa	480	600	-	-	-
Thermal Dilatation coeff.	µm/m-C	23.6x10 ⁻⁶	9x10 ⁻⁶	5x10 ⁻⁶	2x10 ⁻⁶	15x10 ⁻⁶

1.3. Finite elements analysis (FEM)

1.3.1. Fem history

Low thickness structures are, nowadays, the most common type of structures used in all fields from building to vehicle. This is due to the fact that they have an ancient history as background and in the past, the knowledge of their characteristics and their properties permitted the realization of huge buildings like the Roman Pantheon (115-126) and Hagia Sophia (532-537), that exist still now. But, was only in the early '700, during the Renaissance, that scientists point out some mathematical rules to manage these structures that, nowadays, we know as modeling and simulation.

Leonardo da Vinci (1452-1519) with his Codex Madrid I theorized the first model of beam. Further studies were conducted until when Timoshenko, 1953 and Szabo, 1979 pointed out the actual Eulero-Bernulli beam theory.

All these studies aimed to generalize complex tridimensional situations about stresses, forces and reactions into a mathematical equations much more easily to be managed. 2D low thickness structures were be studied by Lagrange (1736-1813), Poisson (1781-1840) and Navier that supplied the correct differential equations. But in these mathematical approach there were some rough analysis, in particular whose correlated to the stiffness constants. Kirchhoff in the early 1800 improve these models and today he is considered as the founder of the modern theory of flat plate.

Furthermore it is really interesting to emphasize how all these studies are started from the same case: vibrational problems. In fact, in 1764, Eulero developed a simulation model for bells, anticipating of about one century many flat plate theories. The need of more accurate solutions bring the development of new theories and mathematical approaches for the entire twenty century. At the beginnings these theories were applied only to buildings and constructions fields but after the industrial revolution they were be applied also to the mechanical, aerospace and biomedical engineering.

Nowadays the informatics capabilities are subjects to a constant evolution that is permitting to apply more and more accurately the FEM method, bringing at the correct solution, saving time and money.

1.3.2. Characteristics and problems related to FEM

Flat structures have a peculiar mechanic characteristic: high resistance in plane and low resistance out the plane. This is also integrated by high values of transversal shear and normal stiffness. Thanks to the growing of computer capabilities and to the high level of customers demand is easy to see how there is the tendency to go to tridimensional analysis. In other words, also the flat structures are simulated by 3D analysis, allowing to recognize all the effects of high order that, in other way, were not possible to be represented by classical flat structures theory.

Another observation that can be done is that the flat structure characteristic is concerned not only to the 3D analysis, but also can be much more complex, for instances showing singularities into the linear elastic analysis not showed into classical models.

Another important aspect that must be take into account is the choice and the interpretation of the correct FEM model. What matter are the basic physical assumptions: if the continuous model is based on the same assumptions, the differences could be appear only by means of a discretization and can be disappear, for instance, by means of a more accurate mesh.

Moreover, stir up high interest the problem of increasing the model order increasing the thickness. It's necessary to define, so, if to use FEM at high or low level: both methods are needful because, maybe, simplest cases could be solved by high order methods; problems with high gradients and discontinuities required formulation at low level. So it is necessary to separate the model type decision from the one referred to the formulation of finite elements: everyone will have errors and approximations that we must be able to recognize and evaluate. At the first phase belong all the simplifications done by continuous model formulation; at the second one will be attributed all those approximation errors that are pointed out by the discretization done during the FEM formulation. While these numerical errors could disappear with a refinement of the mesh, the model imperfections, related to the theory, persist. Distinguish them, represents a crucial point for a further correct results interpretation.

Chapter 2

Instrument model design

2.1. Introduction

This chapters represents the first step of the entire thesis work and it is concerned about the definition of preliminary models. These are modeled with CATIA v5 and are:

- Single smooth plane model;
- Double smooth plane model;
- Single plane model with ribs;
- Double plane model with ribs;

For each model a proper FEM analysis is applied in order to point out important information about model weight, natural frequencies and vibration modes.

2.2. Geometrical parameters definition

The first step was an accurate analysis of the IGS file in order to find the lenses position and to define the correct trajectory of the IR beam.

This trajectory, originally, was sketched by means of twenty parallel lines, reflected by each lens, until they are put away with a precise outlet angle. Since, it is not a so important parameter for this thesis work, it is been decided to represent it by a single beam path obtained by joining, with a straight line, each geometrical lenses center.

So that, as it is possible to see in the [figure 2.1](#), the outgoing beam, that is reflected by a planar mirror angled by 45° , goes out the structure perpendicular to the straight path draws between the last two mirror centers.

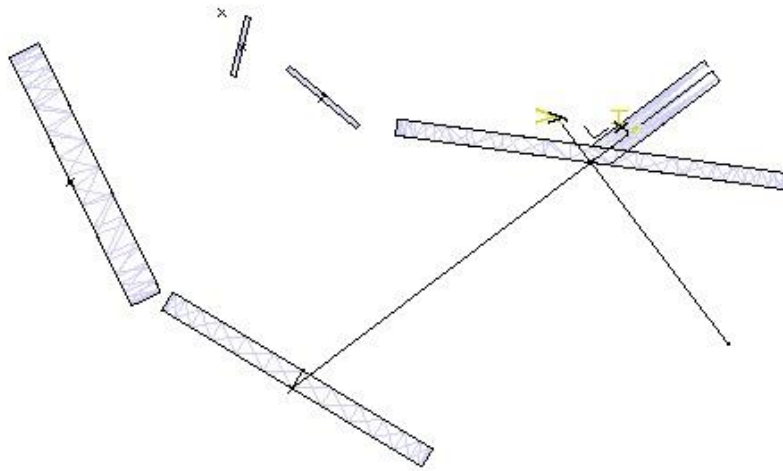


Figure 2.1. *Lenses system and beam path of the first JGO model*

The second step was concerned about the definition of a simple structure, able to containing all the lenses, sensors, motor and all the other instrument parts, with having, at the same time, the minimum dimensions possible.

A particular purpose decided for this preliminary model was that the outgoing IR beam must be perpendicular to a reference plane well defined. This represents only a design constraint that will permits a better managing of the instruments itself during the installation process. Then, it has been necessary to define a relative reference plane for the incoming work.

As just said, in addition to this new practical constraint, others are applied and one of the most important is that the entire finished structure must have a weight less than 5 kg. This means that, during this thesis phase it is necessary to define some maximum and minimum dimension in order to guarantee that all the constraints are respected. Furthermore, all the parts have to be contained into an ideal box with the minimum encumbrance possible.

Looking for relative disposition and dimension of the lenses, it can be say that a simple rectangular shape with length equal to 170 mm and height equal to 120 mm could be the optimum. It has been chosen that the length side represents the reference plane and so it is perpendicular to the outgoing IR beam (figure 2.2).

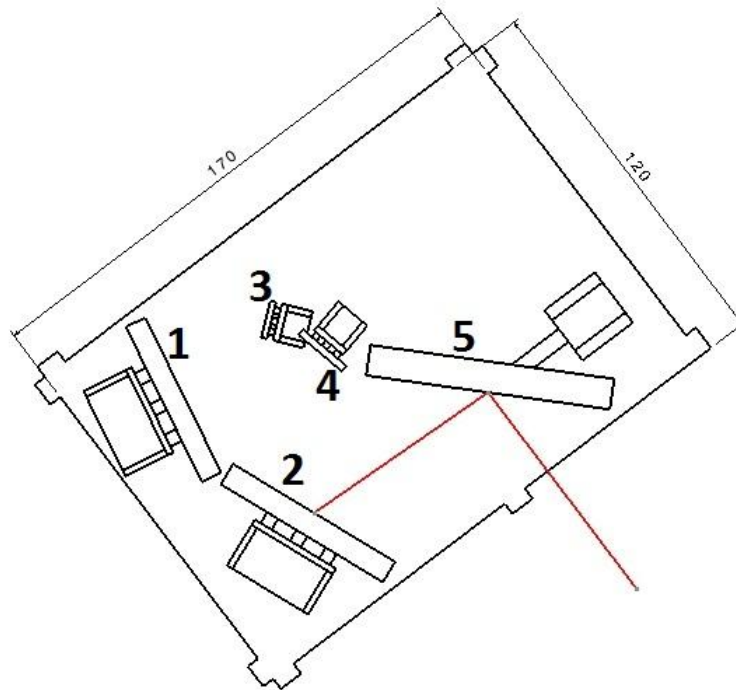


Figure 2.2 *Minimum dimension for the base. The red line represents the outgoing IR beam.*

Figure 2.2 shows four lenses: the lens “5” one that can move by means of an electric motor. The other three lenses are fixed to the base by means of proper supports. An important aspect of these retaining structures is that they have to guarantee the best results, in terms of thermal conductivity and mechanical resistance, with keeping down the weight of the entire instrument at the same time.

To be in agree with what is just said, it has been necessary to design different lens supports in accordance with the kind of lens (dimensions and geometry of it) and with the type of instruments model (with one or two plane structure).

With the exception of the motorized lens, that is a particular case analyzed separately, others lenses supports have one common characteristic. In fact, the problem of an eventual thermal dilatation imposes to design these retain structures so that there will be only three contact point between the lens and its support. In figure 2.3 it is represented the retaining structure adopted for the cases with single plane models.

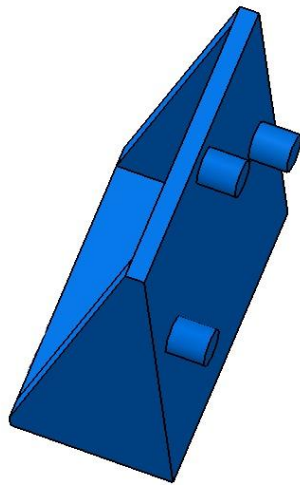


Figure 2.3 *Lens support type 1*

Since the introduction of another plane, orthogonal to the other one, gives the possibility to re-arrange the previous idea of retaining structure, for the lenses number “1” and “2” a new kind of supports is designed. Here a simple pipe with thickness equal to 0.5 mm is adopted and it is schematically represented in the [figure 2.4](#). For each lens are adopted three pipes of the same type in order to assure the respect of the condition of the three contact points.

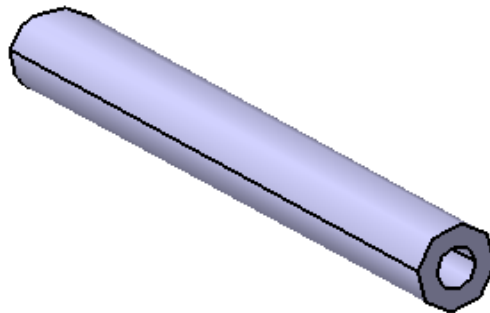


Figure 2.4 *Lens support type 2*

Motorized lens is a particular situation in which the lens need to rotate around the axis that pass through the geometrical center of the lens itself and it is perpendicular to the reference plane adopted. Or, in other way, perpendicular to the outgoing IR beam.

Kind and size of motor are not subject of this thesis and for this reason are here modeled with a simple box with a weight comparable to a possible brushless motor weight. For the same reason, also the motor support, is approximated as rectangular box.

One of the most important part of the entire structure is represented by the instrument supports that permit the assembly with respect to the satellite. A proper design of it must consider that it will be the only part that will be in contact with both instrument and satellite and so, the first structural part that will exchange heat. Furthermore, it has also the important role in giving, to the entire structure, the correct stiffness and mechanical resistance.

In order to guarantee low heat exchange, high stiffness, low mass and resistance at peak load different solutions, for the bench supports, have been taken into account. Knowing that in general, to achieve a high frequency value, it is needed a squat piece instead to long slim one and, considering that, the thermal resistance is increased by the length of the pieces, the evaluation of the bench supports have been made by the two parameters: cross section area and length. After these considerations and looking at the previous cases, studied for other space missions, the solution was to consider tubular v-shaped parts. Controlling the angle, formed by the legs of this type of support, and managing the cross sectional area will possible to obtain a good balance between all discussed design constraints.

In this preliminary thesis phase they are modeled with pipes with thickness equal to 0.5 mm.

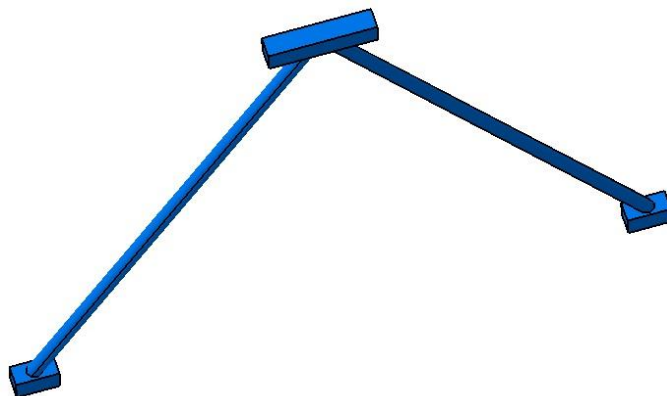


Figure 2.5 *Instrument support*

2.3. FEM analysis' parameters

One of the crucial point of this thesis is the FEM analysis. In order to evaluate in proper way all mechanical parameters, some considerations are necessary. First of all, it must be say that, the analysis is conducted to point out weight and natural frequencies of the model.

Furthermore a comparison between results must be possible and so it's useful to apply some rules in order to have a way to manage and understand them.

Constraints are equally applied between all models. Ground constraints are adopted for instrument supports ([figure 2.6](#)) and simple blocked element constraints is used for all the others parts (see [figure 2.7](#)).

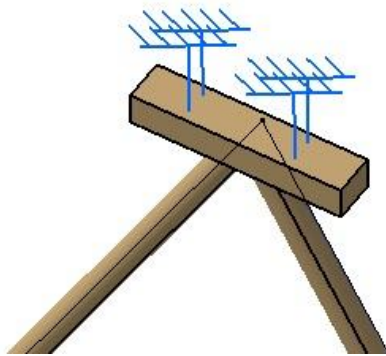


Figure 2.6 *Ground constraint applied to instrument support*

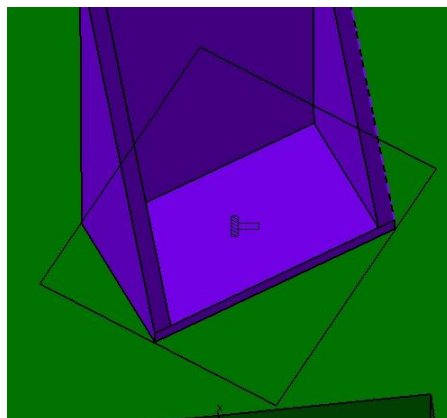


Figure 2.7 *Simple blocked element constraint*

The evaluation of the mesh, dimension and type, is here considered in order to guarantee the results convergence. It has been noticed that good results are obtained for *parabolic mesh* type and with dimension proportional to the one of the elements. The maximum dimension of the mesh is 3 mm and it is associated to the plane. The minimum is 0.8 mm for the lens “4”. Imposing these parameters, results are always convergent to a value of frequency.

Another consideration that can be done is that the parts material used is Standard CATIA Aluminium.

After a preliminary analysis with this material, useful to understand which is the best model in terms of natural frequency and weight, another study has been conducted using Standard CATIA Titanium for some parts. This is due to the fact that the heat exchange is really important and it must be considered. Titanium has insulation properties greater than Aluminium.

2.4. Models design

These models that are presented in the next paragraphs have been analyzed by the FEM analysis considering aluminum as material for all the parts. Clamp constraint have been applied between the instrument supports and the satellite, even if, this represents an overestimating of the results in terms of natural frequency. Connection between the parts have been simulated by a simple clamp condition and also in this case a little overestimation is applied. These overestimation, have been considered only in this first chapter since, at this moment, the main objective was to obtain a preliminary model to be worked in the rest of the thesis.

2.4.1. Single smooth plane model

This model is the simplest one. It is constituted by a smooth rectangular plane with dimensions equal to: 170 mm for the length, 120 mm for the width and 4 mm of thickness.

This model is shown in the following figure ([figure 2.6](#)):

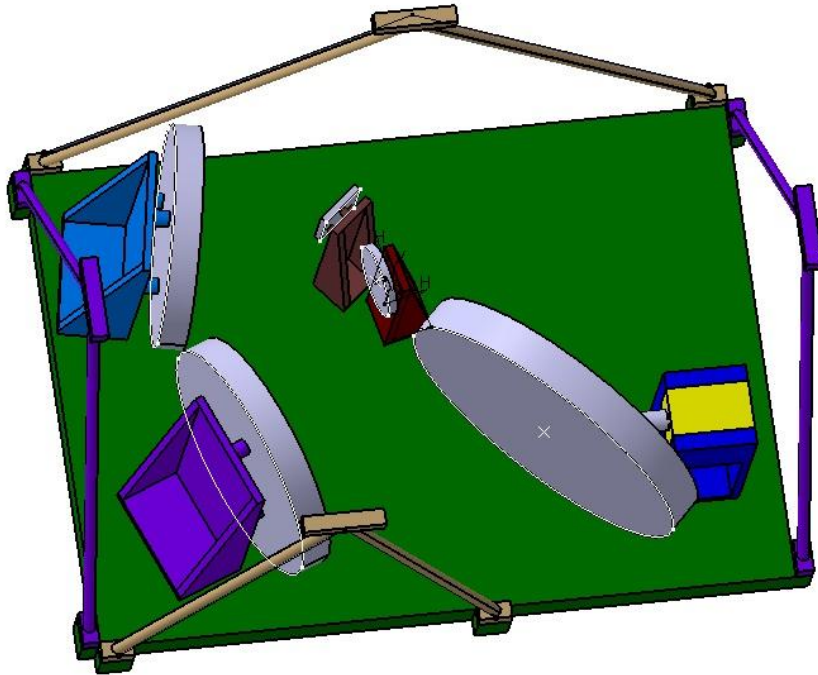


Figure 2.8 *Single plane model*

As it's possible to see all the lenses support facilities are of the first type. No others new model characteristics are introduced here. This model, from a thesis point of view, represents only a starting point for the incoming work.

Mechanical characteristics of this model have been evaluated by means of FEM Analysis. Significant results are summarized in the [Table 2.1](#).

Table 2.1 *Weight and natural frequencies associated to the single plane model. Only the first three vibration modes results are here reported.*

Weight	0.493 kg		
Natural frequency	133 Hz	166 Hz	202 Hz

2.4.2. Double smooth plane model

This other model is built on the basis of the previous one with the addition of a lateral plane with height equal to 60 mm and thickness about 4 mm. This permits to remove the lenses supports type “1”, adopted for lenses 2 and 3, substituting them with the simplest one of type “2”.

Dimensions of the instrument plane are not varied with respect to the previous solution.

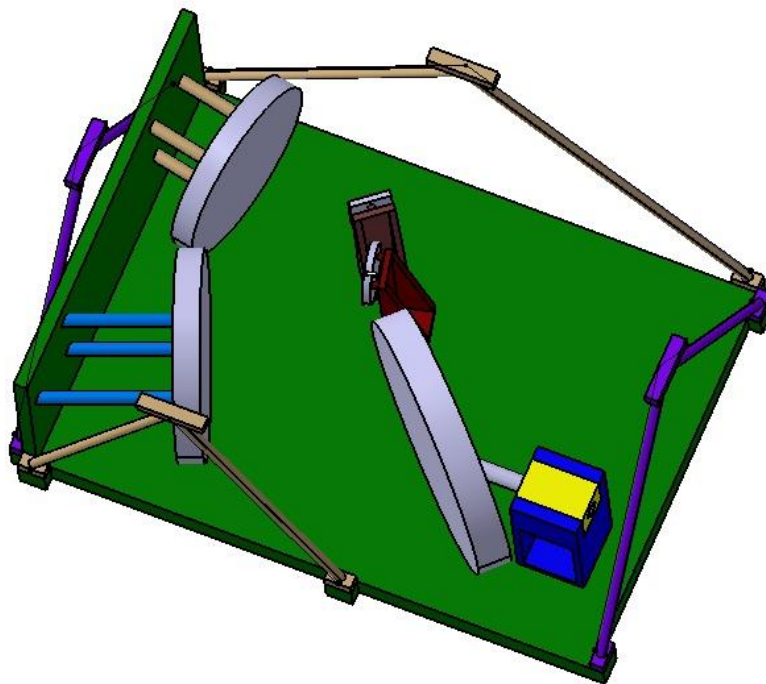


Figure 2.9 *Two plane model*

Results give by the FEM analysis of this model are reported in the [Table 2.2](#).

Table 2.2 *Weight and natural frequencies associated to the double plane model. Only the first three vibration modes results are here reported.*

Weight	0.567 kg		
Natural frequency	120 Hz	139 Hz	161 Hz

In the following we will optimize these two models for reducing the mass without lowering the natural frequencies.

2.4.3. Single plane model with ribs

The optimization of the one-plane-model lead to the layout shown in [Figure 2.8](#). The plate thickness was 4 mm and the ribs patterns were chosen between several different configurations. [Figure 2.10](#) shows the preliminary useful ribs configuration in which height was 6 mm and the instruments plane has now a thickness about 2 mm. Other models with different ribs geometry are not here reported since FEM analysis pointed out worst results.

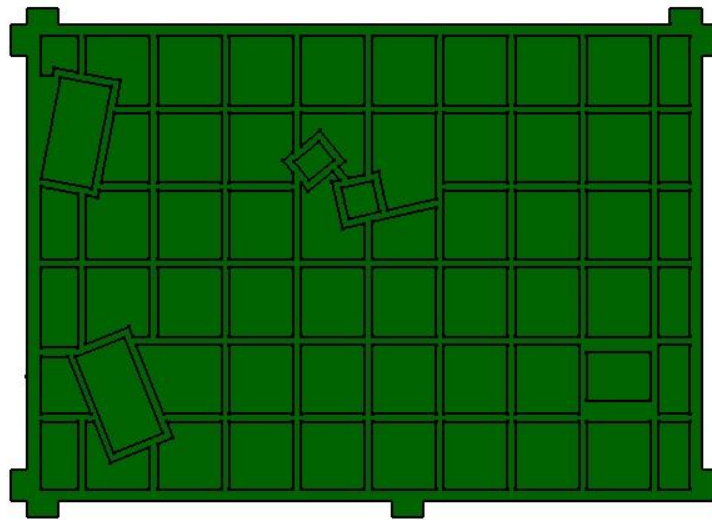


Figure 2.10 *Single plane model with ribs (bottom view)*

[Figure 2.11](#) shows a CATIA's screen capture in which it is possible to see the presence of these ribs (the black lines is the hide pattern, the upper surface is totally smooth) with respect the positions of lenses supports.

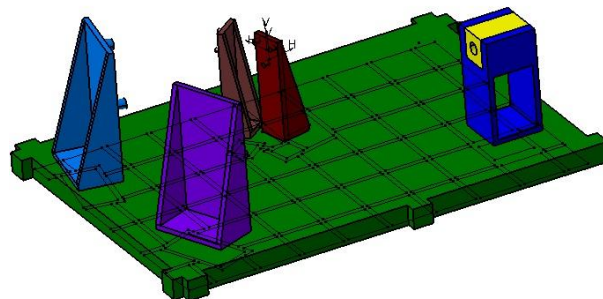


Figure 2.11 *Axonometric view of hide ribs pattern in single plane model*

In the following table are reported FEM's results.

Table 2.3 *Weight and natural frequencies associated to the double plane model. Only the first three vibration modes results are here reported.*

Weight	0.404 kg		
Natural frequency	152 Hz	175 Hz	212 Hz

2.4.4. Double plane model with ribs

Here ribs are introduced also on the second plane but, in this first sketch, the thickness of the second plane doesn't change with respect the original one. So, the starting thickness is equal to 8 mm but the presence of ribs, with height equal to 7,5 mm, permits to reach a value of thickness for the second plane equal to 0,5 mm.

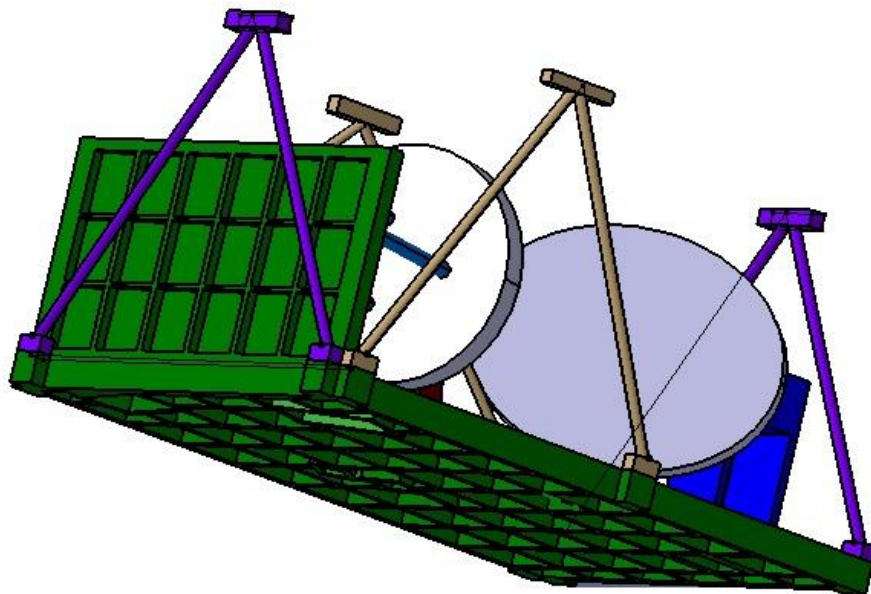


Figure 2.12 *Double plane model with ribs*

Also in this case weight and natural frequencies are reported in the [Table 2.4](#).

Table 2.4. *Weight and natural frequencies associated to the double plane model with ribs. Only the first three vibration modes results are here reported.*

Weight	0.395 kg		
Natural frequency	140 Hz	162 Hz	175 Hz

2.4.5. Consideration about results

By looking at the results, it is possible to see, how the mass changes in the range of values between 0.4 kg and 0.5 kg. The first model (with single smooth plane) and second one (with double smooth plane) are not taken into account since, the single plane does not permit to reach the correct value of natural frequency (which must be greater than 140 Hz) and the other one has the highest value of total mass (0.6 kg) with respect to others models.

The ribbed solutions have a quite similar weight and for this reason the difference, in the choice of the best model, is based on the natural frequency values. Even if the double ribbed plane model has a value of natural frequency equal to 140 Hz, that corresponds to the lower limit, it can be a valid solution since the mass remains low. On the other hand, the model with one single ribbed plane, apart from having a higher value of natural frequency, presents a greater feasibility since it is composed by a single planar surface.

For these reasons the single ribbed plane is the chosen model.

Chapter 3

Optics supports design

3.1. Introduction

This chapter concern about the design of lenses supports. Supports have been initially analyzed with FEM analysis in order to point out the natural frequencies and Von Mises stresses.

The initial point of this chapter is the definition of a nomenclature of the lenses. Figure 3.1 shows the used scheme:

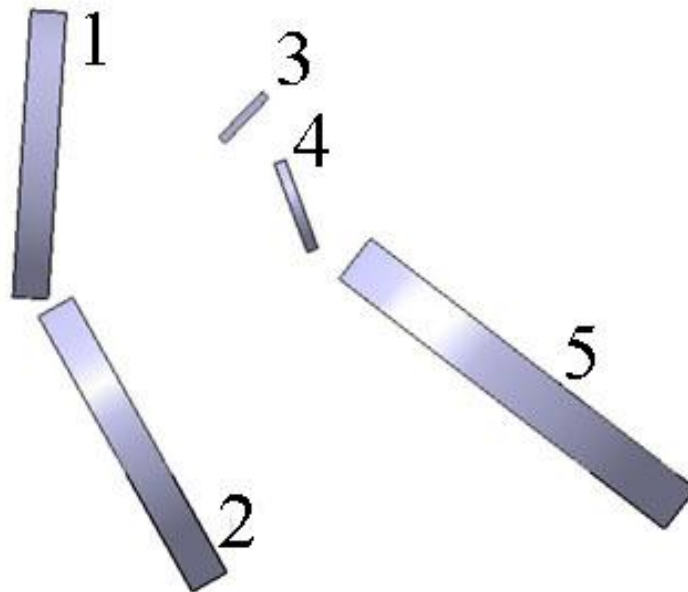


Figure 3.1 *Lenses nomenclature*

Chapter 3

Common consideration equal to all lenses supports can be summarized in these useful points:

1. Lenses and supports, as well as the entire instrument structure, are exposed to an acceleration of 600 m/s^2 ;
2. Lenses are fixed to the instrument base by means three point of contact between supports and lens itself (no details of them are take into account in this thesis work);
3. Lenses supports material is the aluminum alloy Al 7075-T7;
4. Lenses supports are jointed to the base structure by means of austenitic stainless steel screws;
5. The first natural frequency of the single subsystem (lens+support) must be greater than 140Hz. A safely value will be considered up to the twice;
6. The final instruments weight must be as low as possible and this impose that also the parts must give a small weight contribution;

3.2. Lens 1: support model design

3.2.1. First lens support configurations

A first model of lens number one support was sketched in the Chapter 2 with a simple geometry and without real constraints. It is shown in the figure below:

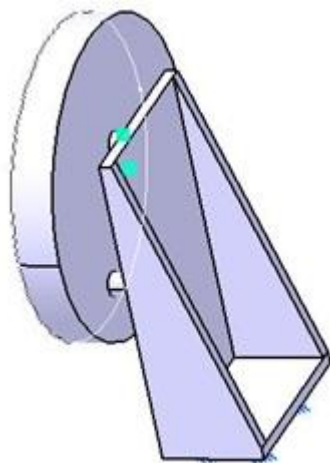


Figure 3.2 *Lens number 1 support. First model*

Instrument base design

This conceptual model has been optimized considering the real constraints given by the screws used to mounting in on the instrument base.

The low weight required for the structure imposes also that the stiffness should be highest possible in order to reach correct value of first natural frequency.

FEM results of this first model aren't reported since they are not useful.

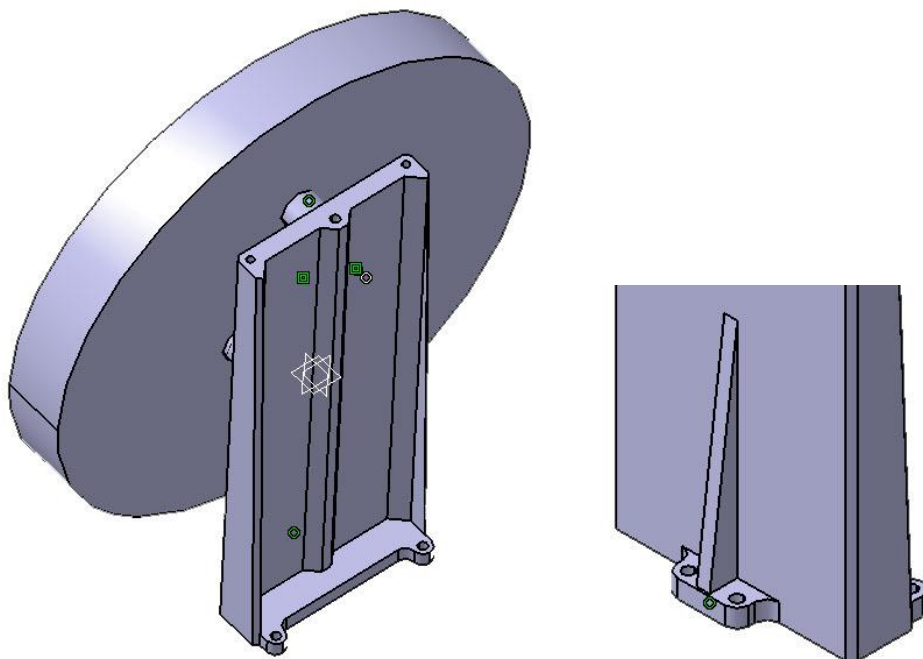


Figure 3.3 *Lens 1 support model with front rib detail.*

In [Figure 3.3](#) new model is characterized by the presence of four holes at the base, two in the front and other two at the back of it. By means of these it is possible to connect the support to the instrument base with screws.

The model weight is about 46 g and thanks to the presence of the frontal rib its first natural frequency is 279 Hz.

This model, seemingly correct, shows some manufacturing problems mainly given by the presence of the frontal rib. This, in fact, could be increase the costs of production without an appreciable increase of model properties.

Another problem could be given by the number of screws. In fact, the presence of the fourth screw add to the structure an hyperstatic constraint. This could be positive or negative. Supposing that this support must be removed temporally and re-mounted, with an hyperstatic solution, may appear some problems related to a non perfect planarity of support surfaces.

But, on the other hand, this additional constraint gives a positive contribution in terms of structure stiffness, increasing it.

The solution with only three screws is then adopted in consideration to the fact that this thesis work is a preliminary study of feasibility. Will be possible to compare, eventually, this solution with another one with four screws.

3.2.2. Lens 1: definitive support model

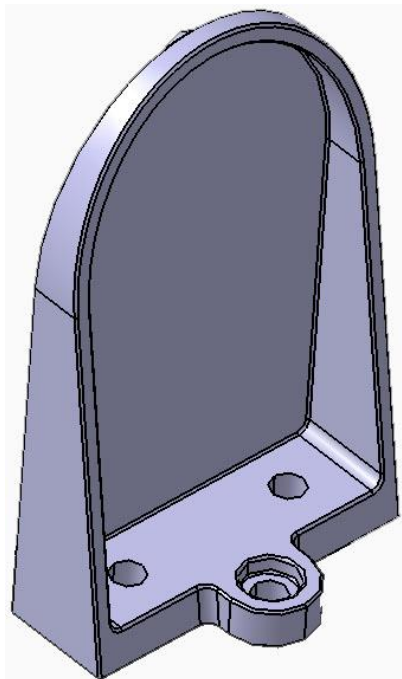


Figure 3.4 *Lens number 1 support model.*

The total weight of this model is about 50 g.

Thanks to a simple drilling cold work it is possible to make three screws holes at the base of the supports. Here, they are modeled with a diameter of 3

Instrument base design

mm except for the third screw that has an hole with two different diameters: 5 mm in order to contain the screw head and 3 mm for the shank.

3.2.3. Natural frequencies analysis



Figure 3.5 *Natural frequencies analysis.*

Values of natural frequencies obtained are reported in the [Table 3.1](#).

Table 3.1 *Natural frequencies*

1 st	466 Hz
2 nd	639 Hz
3 th	941 Hz

As can be seen in this table, frequencies values are higher than the imposed lower limit of 140 Hz. This is a safety decision that may guarantee that the total instrument model will have natural frequency greater than this lower value.

3.2.4. Static analysis

In order to manage all possible critical situation this analysis is conducted considering three cases:

1. Acceleration of 600 m/s^2 applied along z-axis

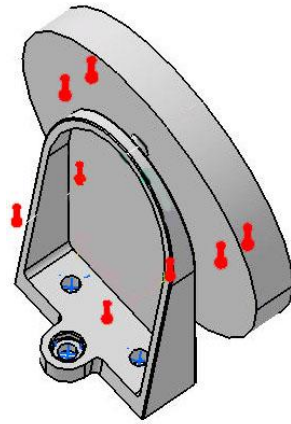


Figure 3.6 Acceleration along z-axis

2. Acceleration of 600 m/s^2 applied along x-axis

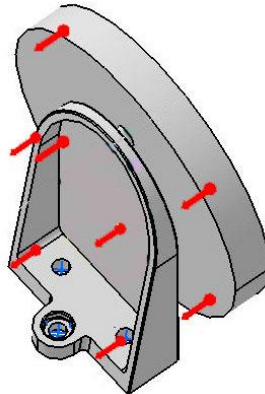


Figure 3.7 Acceleration along x-axis

Instrument base design

3. Acceleration of 600 m/s^2 applied along y-axis

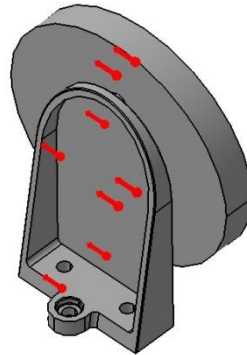


Figure 3.8 Acceleration along y-axis

In the first case, with acceleration applied along z-axis, stress values are in the range between 0 MPa (blue zones) and 15.3 MPa (red zones), see [Figure 3.9](#).

Critical values are reached locally in zones in which there is the presence of rough edges. This effect can be controlled, easily, with rounding off these parts.

However the maximum stress reached in this load condition of about 15 MPa is lower than the admissible limit of the chose material that is safely imposed at 400 MPa.

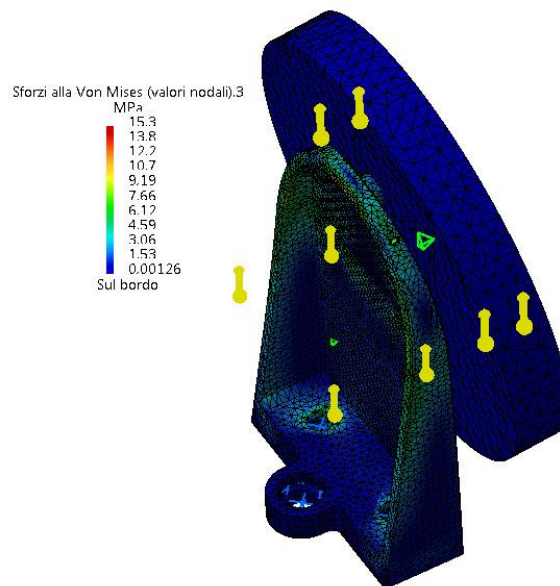


Figure 3.9 Static FEM Analysis. 600 m/s^2 along z-axis direction

Chapter 3

In the case of acceleration acting along y-axis the stress trend is showed in Figure 3.10:

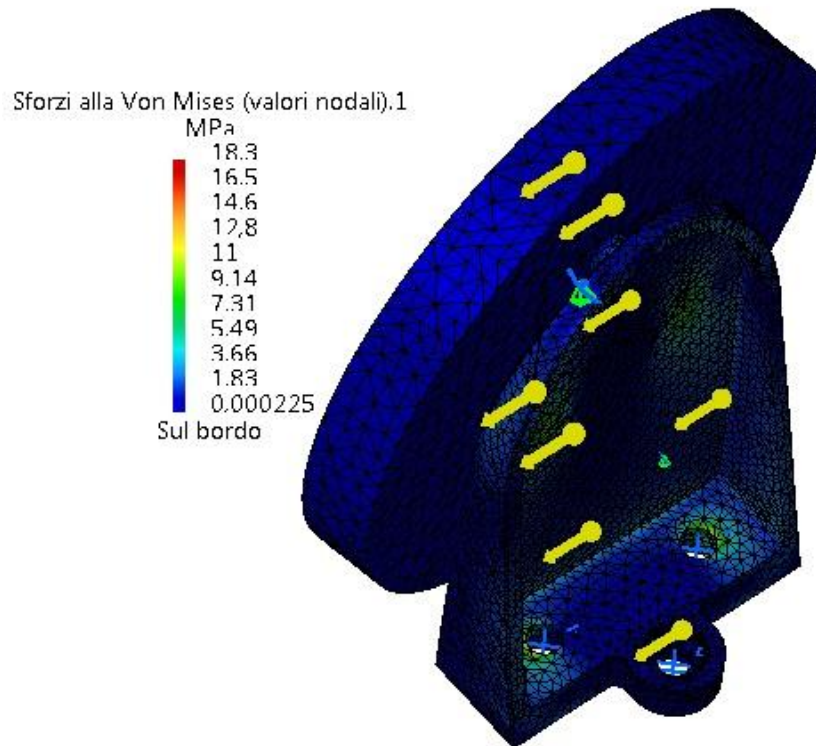


Figure 3.10 Acceleration acting along y-axis

As it is possible to see stress value is not so far from the one reached in the case of acceleration acting along the z-axis. The maximum value is 18 MPa.

In the other case acceleration acts along the x-axis. In Figure 3.11 it is possible to see that in this situation there are higher value of stress than the previous one. Maximum value of stress is now about 41.5MPa.

Also in this case the maximum stress is achieved in regions in which there are rough edges and, for the same reasons of before, perfectly reducible with an accurate rounding off of the parts.

Instrument base design

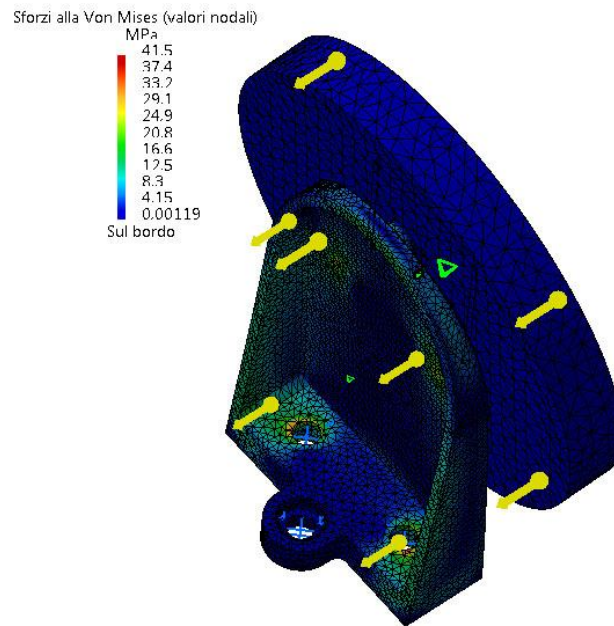


Figure 3.11 Static FEM Analysis. 600m/s^2 along x -axis direction

The maximum stress, furthermore, also in this case is lower than the admissible value of the material, as just said, imposed to 400 MPa.

Material resistance is evaluated by means of MOS coefficient [7]. Since it is evaluated in the yield point the *Factor of Safety* (FOS) have been imposed at 1.25. The value of the Margin of Safety (MOS) must be greater than 0:

$$MOS = \frac{\text{Allowable Load}}{\text{Applied load} * FOS} - 1 = \frac{400 \text{ MPa}}{42 \text{ MPa} * 1.25} - 1 = 6.62 > 0$$

That is strongly verified.

3.3. Lens 2: support model design

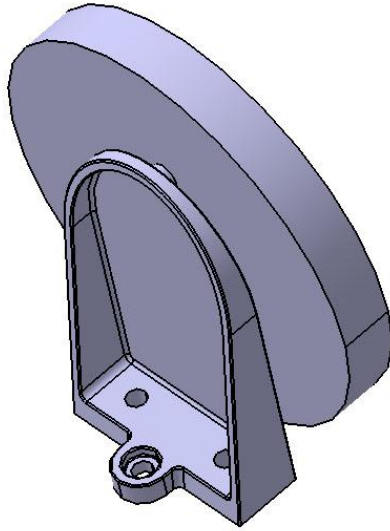


Figure 3.12 *Lens 2 support model.*

In [Figure 3.12](#) is possible to see that the lens number 2 model is the same adopted for the lens 1. This is due to the fact that the two lenses are quite similar. Since this new lens has a weight greater than the other one, the total model mass is increased and reaches a value of about 70 g.

3.1.1. Natural frequencies analysis

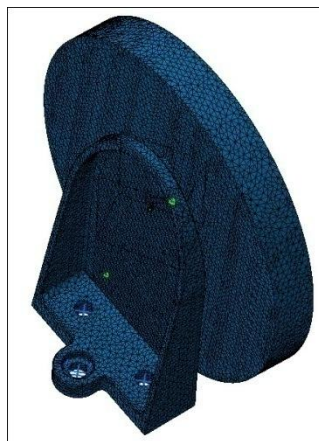


Figure 3.13 *Lens 2 support frequency analysis.*

Instrument base design

Result of this analysis are reported in [Table 3.2](#).

Table 3.2 *Natural frequencies*

1 st	360 Hz
2 nd	491 Hz
3 th	736 Hz

3.1.2. Static analysis

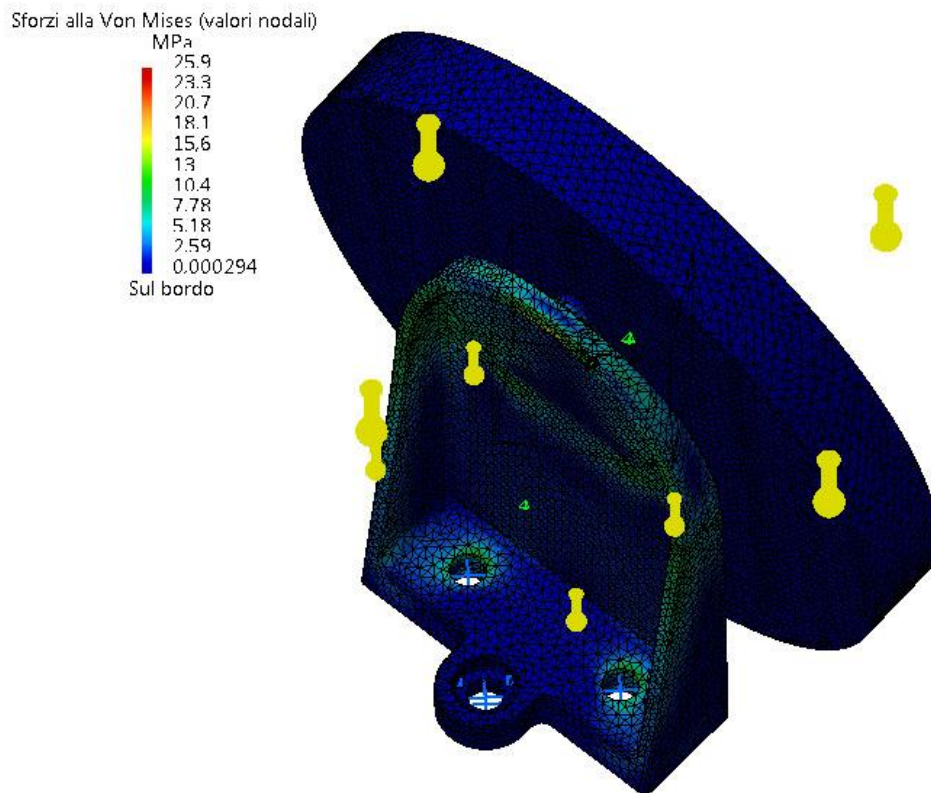


Figure 3.14 *Static analysis with 600m/s^2 applied along z-axis.*

The case showed in [Figure 3.14](#) represents the situation in which acceleration acts along the z-axis and can be noticed that the maximum value reaches by the stress is about 26 MPa. The minimum is 0MPa.

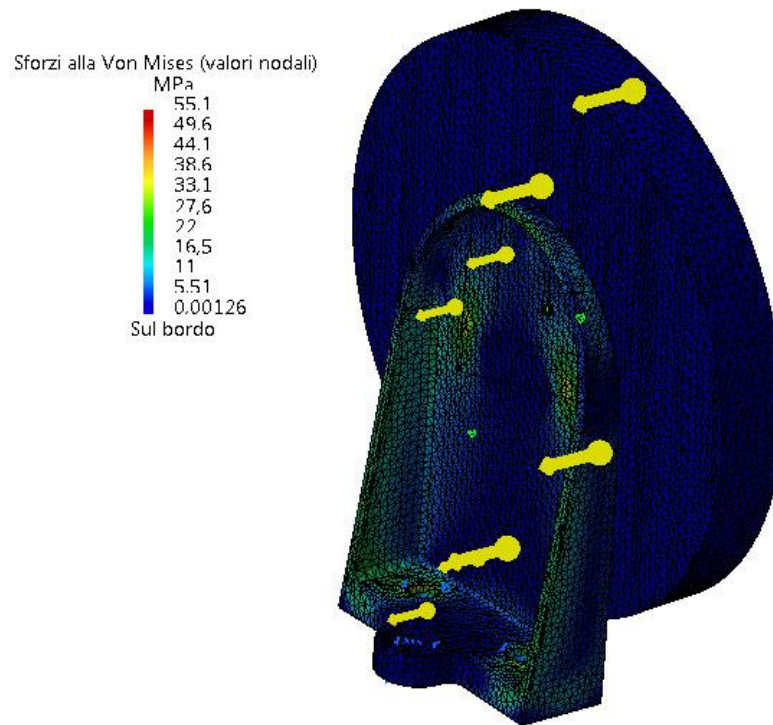


Figure 3.15 Static analysis with 600m/s^2 applied along x-axis.

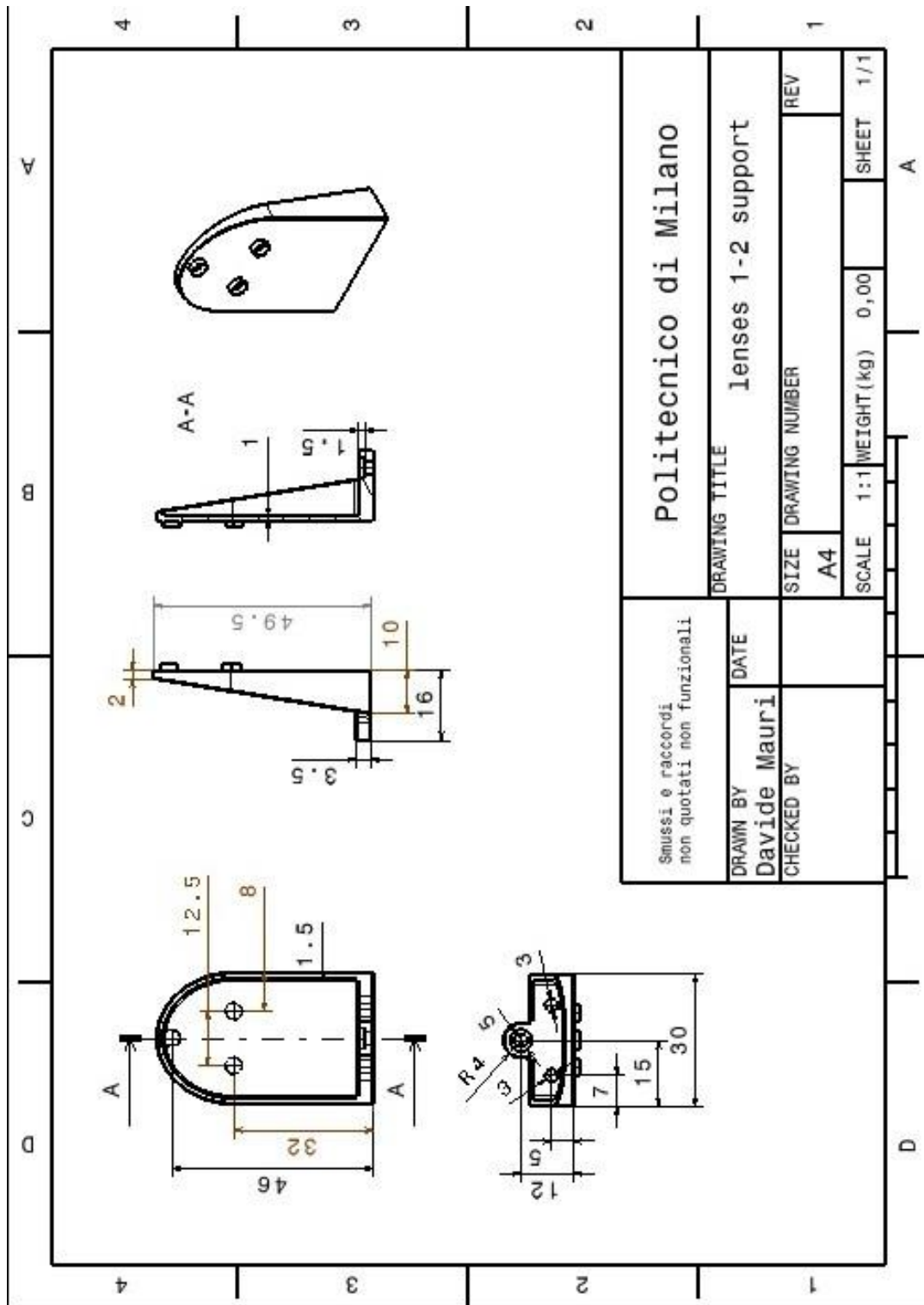
The other case proposed in [Figure 3.15](#) is the one in which the acceleration acts along the x-axis. The maximum stress is about 55 MPa. In all of the two cases the maximum value reached is lower than the material limit.

The case in which the acceleration acts along the y-axis, as the case before, does not give an important contribution so, the results in this case are not here reported.

The value of the Margin of Safety (MOS) [7] is evaluated for the worst condition reached for the case in which the acceleration acts along the x-axis:

$$MOS = \frac{\text{Allowable Load}}{\text{Applied load} * FOS} - 1 = \frac{400 \text{ MPa}}{55 \text{ MPa} * 1.25} - 1 = 4.82 > 0$$

Instrument base design



3.4. Lens 3: support model design

The first configuration of lens 3 (and lens 4) supports have been obtained scaling the one adopted for the previous cases (lenses 1 and 2).

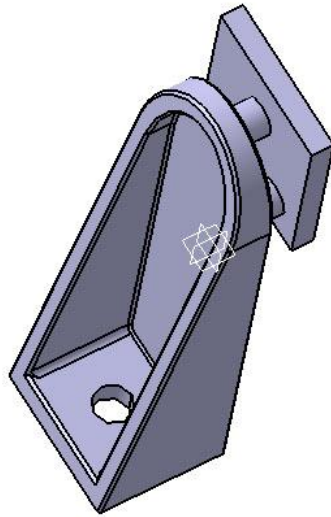


Figure 3.16 *Lens number 3 support.*

The difference of this supports, with respect to others, is the presence of only one screw at its base. Since this part must be connected to the base of the instrument with high precision and since the only one screw does not permit to obtain an accurate and safely mounting, this model is implemented with two pins at the base. This part, showed in [Figure 3.15](#), is roughly modeled here since its characteristics are related to the ones of the instrument base. Within the modeling of the other parts will be possible to analyze accurately also this solution.

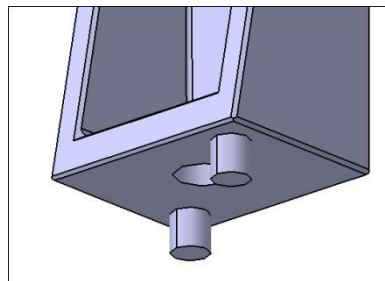


Figure 3.17 *Lens 3 support base pins.*

3.4.1. Natural frequencies analysis



Figure 3.18 *Lens 3 support under FEM investigation.*

Values of natural frequency are reported into the Table 3.4.

Table 3.3 *Natural frequencies*

1 st	1878 Hz
2 nd	2138 Hz
3 th	5434

3.4.2. Static analysis

Static analysis is conducted in order to point out problems due to the application of an external load. In our case this force is represented by an acceleration of 600 m/s^2 that is considered acting separately in two direction: along z and x axis.

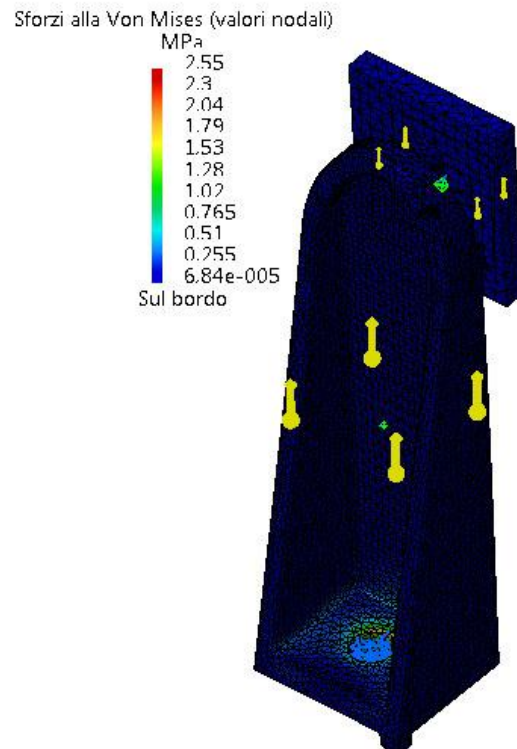


Figure 3.19 Acceleration applied along z-axis direction

As it's possible to see in [Figure 3.17](#) the effect of the imposed acceleration does not bring the structure to dangerous condition in terms of stresses. The maximum critical value is reached at the value of only 2.55 MPa that is very far from the material limit of 400 MPa. Furthermore it is reached at the contact point between the screw head and the support base. Considering an accurate rounding off operation to that edge, may will be possible to reduce also this value.

The other case analyzed is the one that consider the acceleration acting along x-axis. [Figure 3.18](#) shows the static analysis conducted by means of CATIA.

Instrument base design

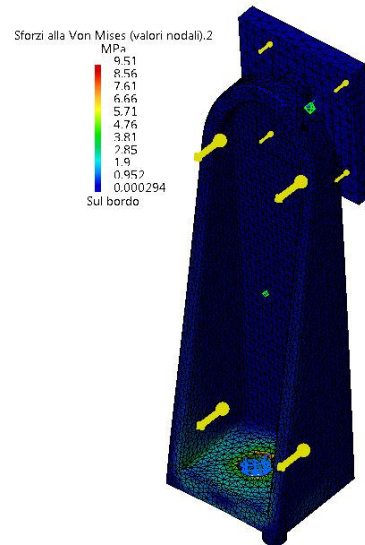


Figure 3.20 Acceleration acting along x-axis.

In this case the value of stresses are incremented a little bit than before but no limit extremes are reached. Maximum value is about 10 MPa that is forty times lower than the critical one. Also in this case it is reached in correspondence of a rough edge.

In Figure 3.21 is showed the case in which the acceleration acting along the y-axis gives a maximum stress value of 9 MPa.

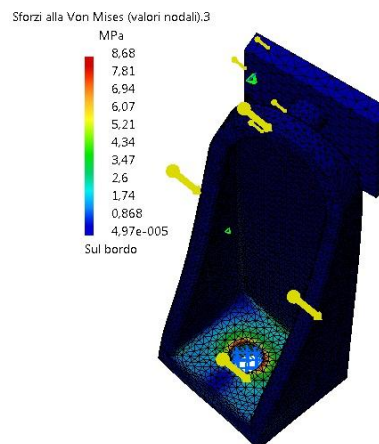


Figure 3.21 Acceleration acting along y-axis

3.5. Lens 4: support model design

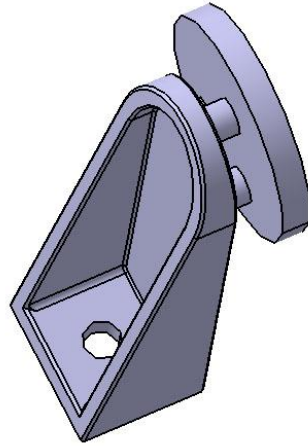


Figure 3.22 *Lens 4 support model.*

Also in this case the support adopted for this lens is the same of the case of the lens 3. Here the weight is 5.91 g.

3.5.1. Natural frequencies analysis



Figure 3.23 *Lens 4 support model.*

Instrument base design

In Table 3.4 are summarized the first three natural frequencies related to the lens support.

Table 3.4 *Natural frequencies*

1 st	1578 Hz
2 nd	1874 Hz
3 th	4086 Hz

3.5.2. Natural frequencies consideration

Natural frequencies value, in all cases, were high and could be lowered by reducing the stiffness that can be achieved by reducing the wall thickness. The main problem, in this case, could be represented by the feasibility of the part with a wall thickness too much thin.

For this reason, after a valuation of the feasibility, it have been chosen to maintain the configuration proposed in 3.4 and 3.5 paragraph.

3.5.3. Static analysis

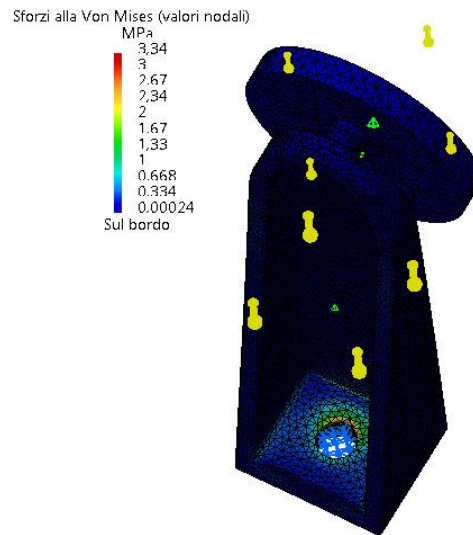


Figure 3.24 Static analysis with $600m/s^2$ applied along z-axis.

Result of static analysis gives that the maximum value is equal to 4 MPa when the acceleration acts along the z-axis (Figure 3.24) and about 12 MPa when acts along the x-axis (Figure 3.25).

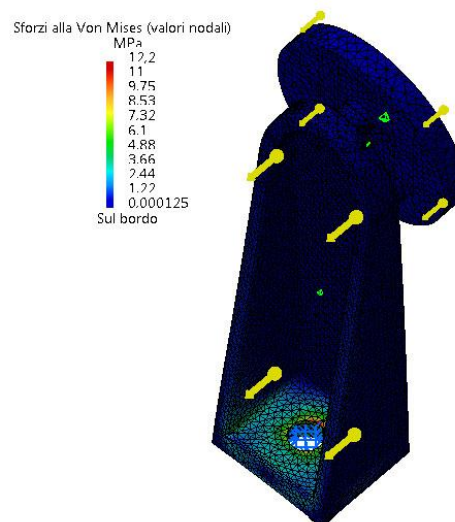


Figure 3.25 Static analysis with $600m/s^2$ applied along x-axis.

Instrument base design

In case in which the acceleration acts along the y-axis the situation that can occurs is showed in Figure 3.26. Maximum value of stress is 11 MPa.

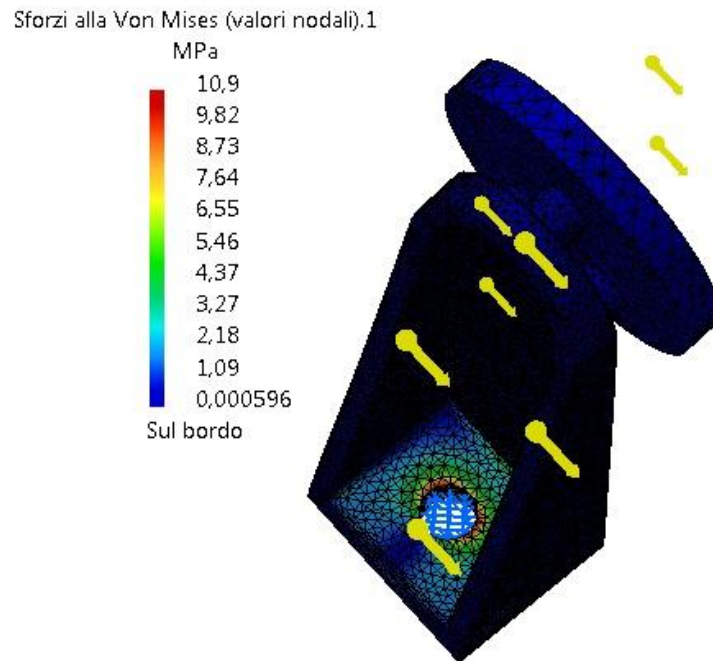
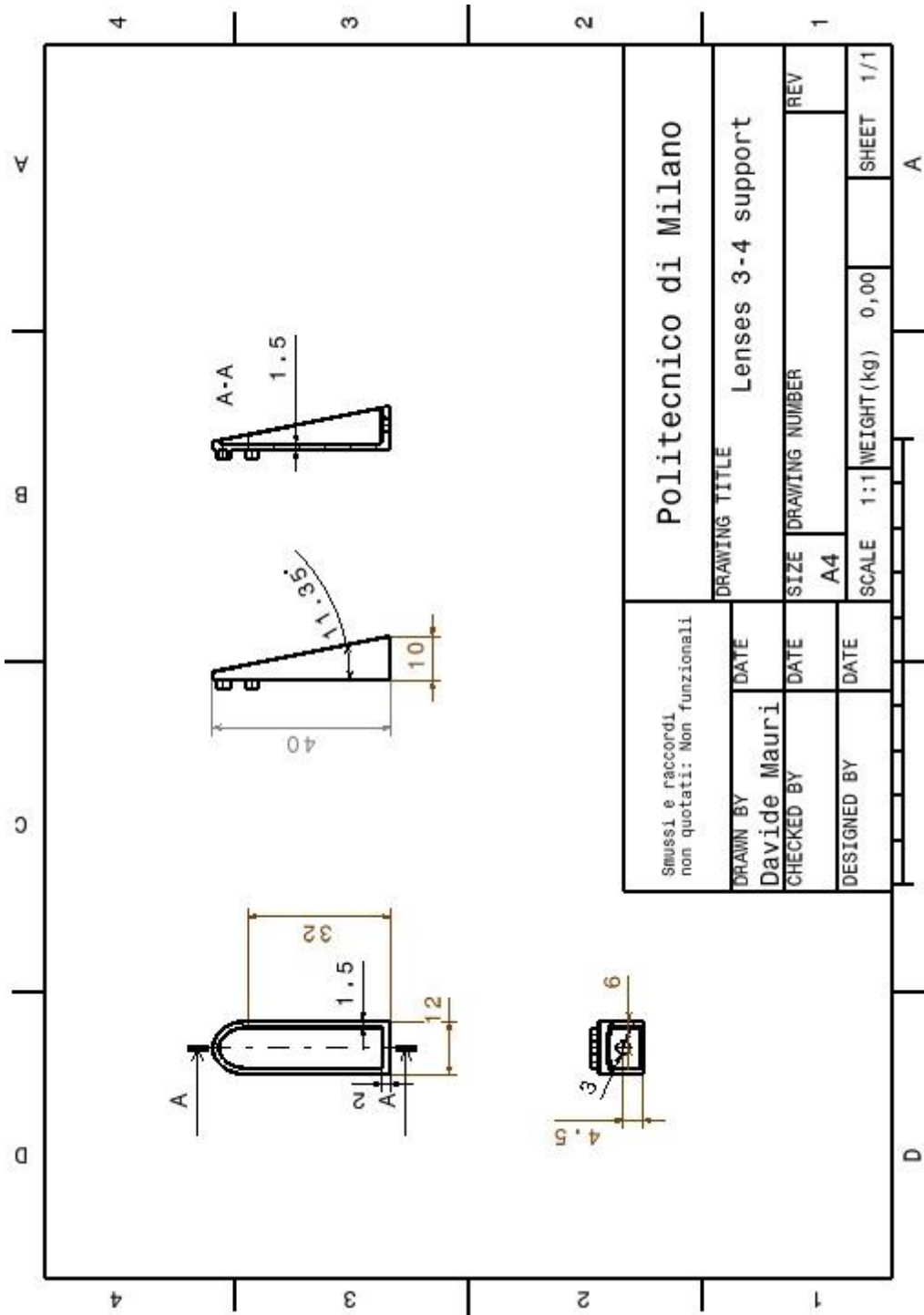


Figure 3.26 *Acceleration acting along y-axis*



3.6. Alternative solution for lenses 3 and 4 supports

Considering that the value obtained for natural frequency is, in both the cases (lenses 3 and 4), a high value and, moreover, the Von Mises analysis pointed out low values stresses, the presence of the ribs could be deleted obtaining an alternative model. [Figure 3.27](#) shows the newest solution characterized by low mass (4 g) and by a value of natural frequency equal to 800 Hz. This new model has height equal to 40 mm, base length of 10 mm and a constant thickness equal to 2 mm .

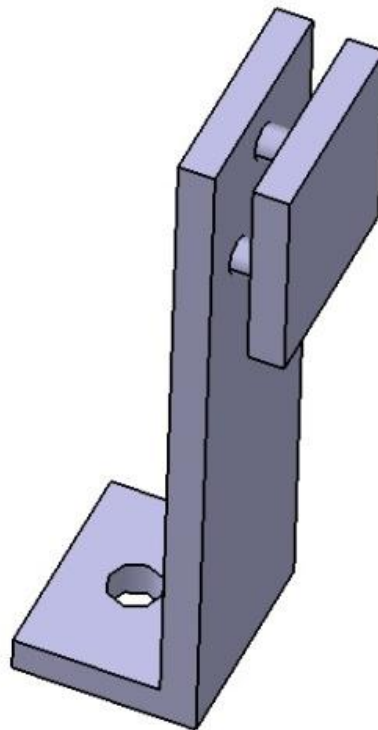


Figure 3.27 Modified model for lens 3 support

The worst condition in terms of stress for this new model is reached when the acceleration acts along the x-axis. In [Figure 3.28](#) it is possible to see the result of these preliminary study.

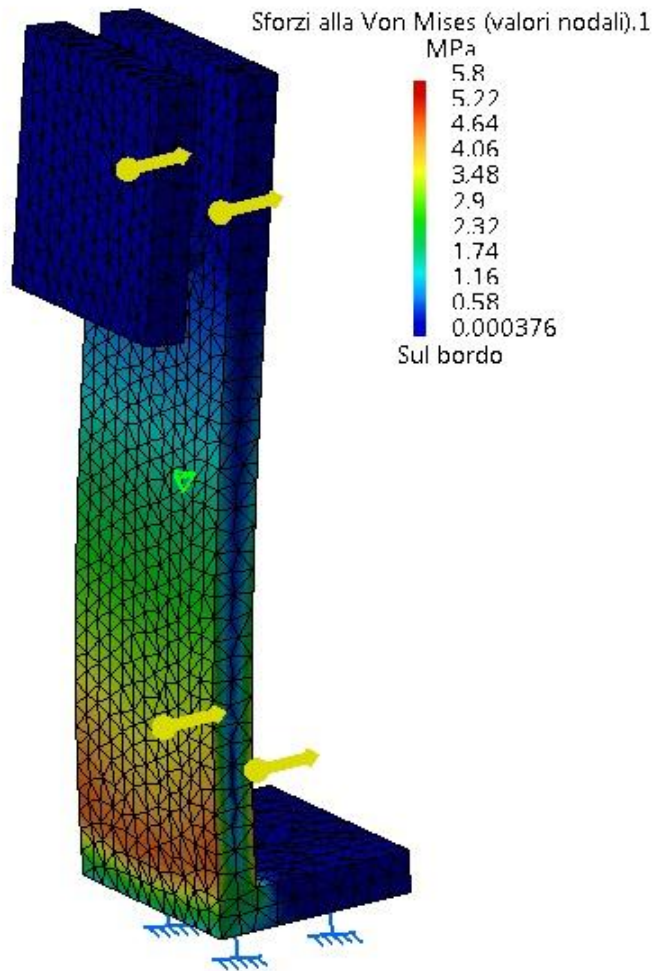


Figure 3.28 Static analysis on modified lens 3 support

As it is possible to see in [Figure 3.28](#), the maximum stress condition is reached at the support base and it is equal to 6 MPa. Thanks to these values, frequency, mass and stresses this rough model could be the best solution; a further analysis could bring to the definitive solution reducing, for instance, the mass locally where is not needed.

But, since this thesis takes into account that some changes to lenses dimensions could be applied in future (with the definitive instrument model) and, also since no real lenses mounting systems have been studied, it has been preferred to use models presented in paragraph 3.4 and 3.5.

3.7. Lens 5: support model design

The design of the support of this optic is the topic of another thesis work and, so, will not be deal-with here.

3.8. Screws design

In this thesis, screws, have been designed in accordance with CNR UNI 10011 standard.

The first step is to evaluate effects of the load, represented by the inertial force provided by the imposed acceleration, to the constraints addicted by the screws.

Using the constraint sensors function of CATIA is possible to evaluate the resultant force at which screws are subjected. All lenses support were analyzed in order to point out the maximum value of resultant force at which screws are called to operate taking into account the two situation: with acceleration along z or x axis.

The worst condition is verified in the case of the lens number 2 in which the inertial force gives a constraint resultant equal to 24 N when the acceleration is applied along x-axis.

Data:

Load: $F_c=24$ N

Number of contact planes: $n_c=1$

Screws type: UNI 5931 M3

Resistance class: 8.8

Diameters: $d_n=3$ mm

$A_{res}=7,06$ mm²

Functional characteristics:

Sliding reduction coeff.: $\gamma_f=1.25$

Friction coeff.: $\mu=0.61$

Chapter 3

Screws safety coeff.: $v_s=1,5$

Referring to the CNR UNI 10011:88 it is possible to define some parameters.

Resistance characteristics:

Screw limit strain: $f_{k,N}=560 \text{ N/mm}^2$

Screw admissible strain: $\sigma_{adm} = \frac{f_{k,N}}{v_s} = \frac{560}{1,5} = 373 \text{ N/mm}^2$

Force transmissible by friction: $V_{f,0} = \frac{\mu * N_s}{\gamma_f}$

Tensile force due to tightening: $N_s = 0.8 * A_{res} * f_{k,N}$

No sliding limit condition: $V_{f,0} \geq F_c$

So, it is possible to define the value of minimum resistance area requested for the screw:

$$A_{res,min} = \frac{\gamma_f * F_c}{\mu * 0.8 * f_{k,n}} = 0.110 \text{ mm}^2$$

By means of UNI 4535:64 it is possible to choose a screw in order to guarantee the condition: $A_R \geq A_{res,min}$:

$$A_R = \frac{\pi}{4} * \left(\frac{d_2 + d_3}{2} \right)^2$$

Table 3.5 UNI 4535

	d₂ [mm]	d₃ [mm]	Ar [mm²]
M3	2.874	2.580	8,48

And so, obviously the chosen screw [11] is verified.

Table 3.6 *Characteristics of the screw UNI 5931 - M3*

Material		Stainless Steel
Thread	Tolerance	6g
	Normative	UNI 4534 (= ISO 261), UNI 5541 (= ISO 965)
Mechanical Characteristics	Resistance class	defined into UNI 7323 / 8
Surface		Natural or designed into UNI 3740 / 6

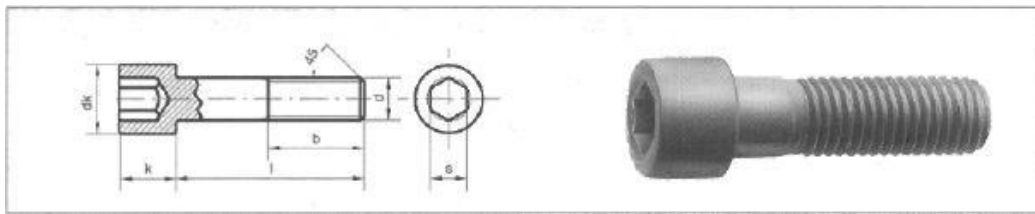


Figure 3.29 *Screw*

3.8.1. Screw design for other parts

Screws that are verified in the previous paragraph represent the worst condition possible so, after an evaluation, it is possible to say that also other screws adopted for lenses supports are verified.

Chapter 4

Optical bench design optimization

4.1. Introduction

Starting from the preliminary analysis of Chapter 2, and using the actual lenses supports masses it is possible to define a new instrument optical bench.

In order to reach the correct value of natural frequency (imposed at a value larger than 140 Hz) and to limit the instrument mass, an accurate analysis of ribs geometry was performed.

The study of the optical bench described in this chapter considers a preliminary (and not optimized) geometry of the links with the satellite and, consequently, will require a successive validation in Chapter 5.

4.2. Optical bench ribs optimization

4.2.1. General plane dimensions definition

In Chapter 2 minimum dimensions of the instrument optical bench were fixed to 120 mm x 170 mm (see Figure 2.2). After the optics supports design Chapter 3, these dimensions can be refined.

The critical point was represented by the presence of the electric motor that is the topic of another thesis, performed in parallel with this one. The design of the motor evolved to a new configuration that can be summarized with a box with dimensions about 120x110x80 mm and with weight equal to 400 g. The optical bench layout has therefore to be enlarged as shown in Figure 4.1

With respect to the study until now conducted, new plane dimensions are showed in the figure below:

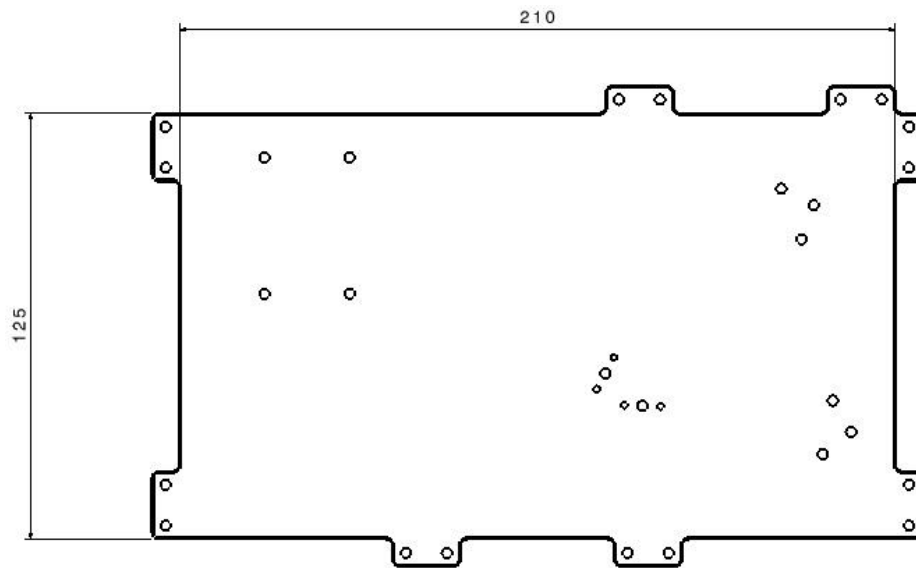


Figure 4.1 *Definitive dimension for instrument base*

4.2.2. Ribbed plane design

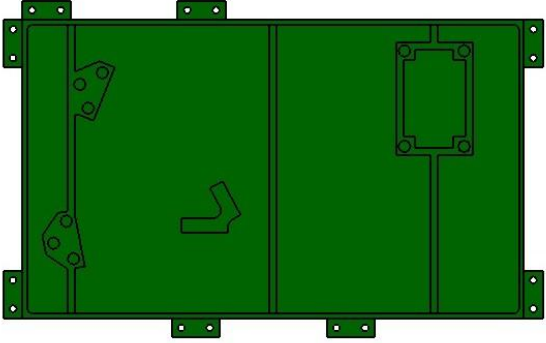
In this preliminary study phase of the instrument plane design some configuration of ribs pattern are taken into account. Starting from the simplest solution and by means of FEM analysis have been pointed out some positive results in terms of natural frequency and model weight. In [Table 4.1](#) are shown some of the most important results obtained.

These models have some common geometrical characteristics like the ribs width, fixed at 3 mm, and the thickness of the principal plane imposed at 0.7 mm. Furthermore, the material used for this part is the same adopted for all the parts modeled until now, that is Aluminium.

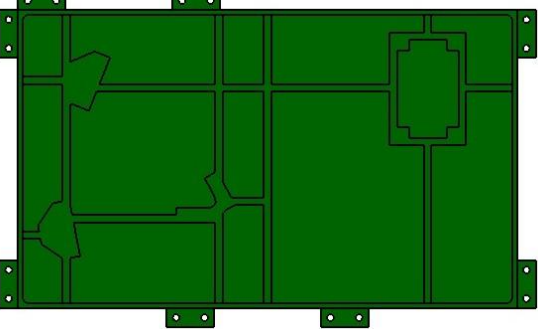
These models, [Table 4.1](#), have been analyzed by means of constraints in which rotational and translational degrees are blocked. This is due to the fact that until now no real constraints can be applied since no instrument base supports have been modeled, yet.

Table 4.1. Ribs pattern analysis

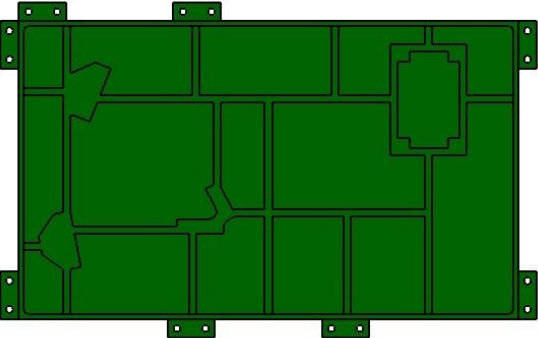
Model n° 1

	Mass [kg]	N.F. [Hz]	Ribs heigh [mm]
	0.1	119	2
	0.103	135	3
	0.109	151	4

Model n° 2

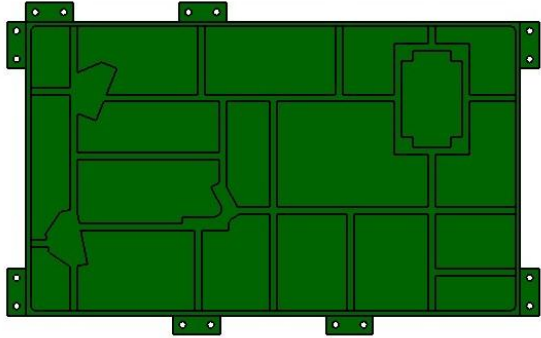
	Mass [kg]	N.F. [Hz]	Ribs heigh [mm]
	0.103	134	2
	0.111	160	3
	0.12	184	4

Model n° 3

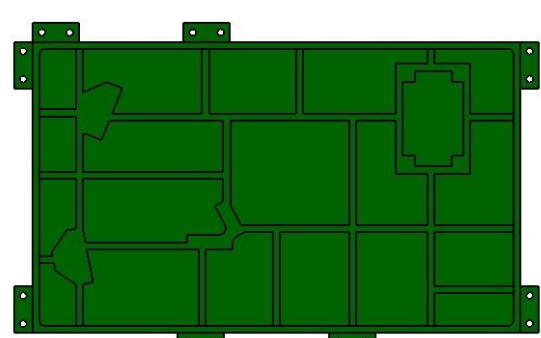
	Mass [kg]	N.F. [Hz]	Ribs heigh [mm]
	0.104	141	2
	0.114	170	3
	0.123	195	4

Chapter 4

Model n° . 4

	Mass [kg]	N.F. [Hz]	Ribs heigh [mm]
	0.106	148	2
	0.117	182	3
	0.128	212	4

Model n° . 5

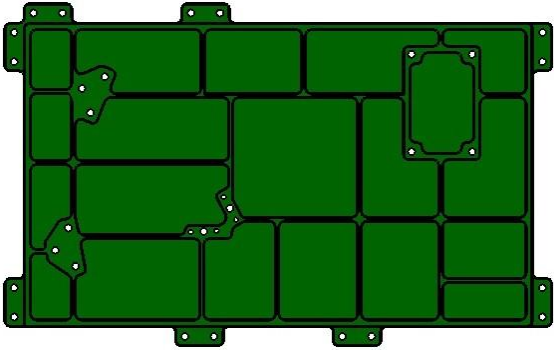
	Mass [kg]	N.F. [Hz]	Ribs heigh [mm]
	0.116	171	2
	0.127	207	3
	0.137	237	4

These last model has been usefulness to reach the quasi definitive configuration showed in the [Table 4.2](#). In this new model some changes have been applied. First of all, the principal plane thickness is reduced at 0.5 mm and the ribs width is now about 2 mm while its height is increased at 6 mm.

Since no instrument base supports have been modeled yet, this model is constrained by means of hinges with rotational degree blocked.

Table 4.2 *Quasi definitive model*

Model n° 6

	Mass [kg]	N.F. [Hz]	Ribs heigh [mm]
	0.139	252	2

Chapter 5

Optical Bench Supports

5.1. Introduction

This chapter describes the design of JGO instrument optical bench supports starting from the configuration defined in [Chapter 4](#). As previously mentioned in [Paragraph 2.2](#), instruments supports must provide a rigid link between the instrument and the satellite frame with a high thermal resistance. The preliminary study of [Chapter 2](#) was based on V-shaped links similar to the ones shown in [Figure 5.1](#). These structures are compliant in the direction that is perpendicular to the plane that contains the three points, but are definitely rigid in the in-plane direction. Consequently, their selectively compliant behavior allows designing highly hyperstatic links that do not suffer from the different CTE of materials.

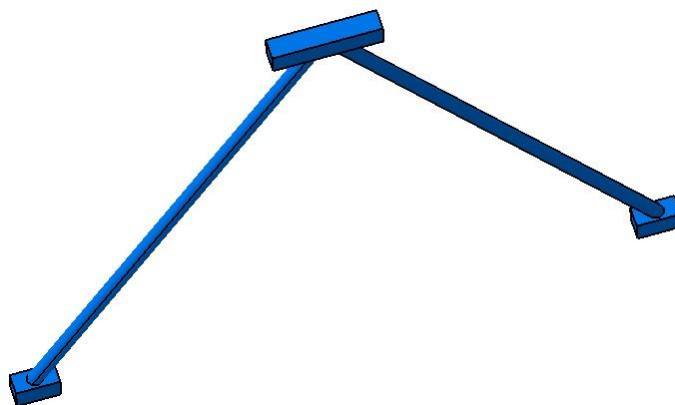


Figure 5.1 *JGO Instrument base support*

Chapter 5

The preliminar JGO model that has been proposed in [Chapter 2](#) is showed in [Figure 5.2](#). This preliminary solution, was based on the simplified optical bench and, consequently, must be updated.

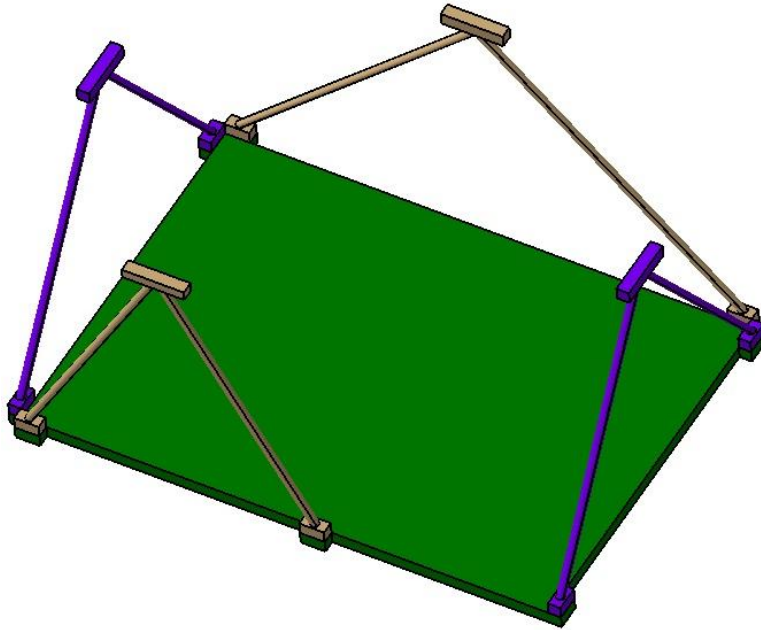


Figure 5.2 *First rough situation for JGO Instrument base support*

Two analyses were performed on supports: peak load and thermal analysis. The first one is necessary since these parts are composed by long slim tubes. The second analysis is important to guarantee a low heat exchange between instrument base and satellite. These analyses allowed determining the best solution minimizing the thermal conductivity and, obviously, the mass.

5.2. Geometry of the supports definition

Owing to the natural frequency constraint, the geometry definition of the supports required an accurate design. Furthermore, the design of these parts affects the design of the optical bench (the same natural frequency could be reached with stiff links and rather compliant optical base or vice-versa). In particular what can really affect the natural frequency is the angle between the two linear tubes. This angle is limited by the instrument geometry and has to be verified in peak load condition.

5.3. Peak load analysis

5.3.1. Eulero theory

When is take into account the study of compressed pieces it is possible to find the equation $\sigma=P/A$ that, as it's possible to see, does not depends on the length of the considered body. Obviously, this contrasts with the experience; perhaps, as it is possible to see in [Figure 5.3](#) two situations can occurs:

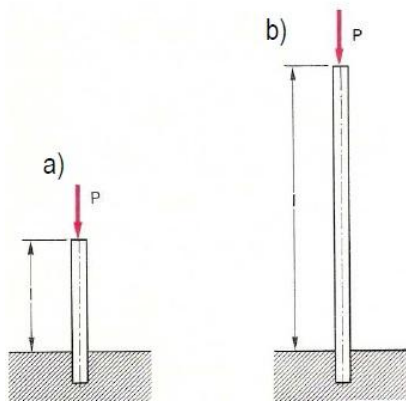


Figure 5.3 a) Squat bar. b) Long length bar

In the case b) the length is higher than the transversal dimension and so, may be, under the load condition it is possible that the momentum will increase with the deformation. For this reason, the compression analysis is not useful since another condition is happening and it is called “peak load” situation.

Chapter 5

It is obviously that, at the external momentum $M_e = P \cdot e$, the bar will oppose, by an elastic reaction, an internal momentum M_i , sum of momentum of the single bending strain σ , that, if it is greater than M_e straighten up the bar after the removal of the load.

To decide if to take into account or not the “peak load” condition it is useful to evaluate the slinness λ of the bar that depends on two parameters. The first one is the minimum inertial radius i_{min} of the section A of the bar:

$$i_{min} = \sqrt{\frac{I_{min}}{A}}$$

Where the I_{min} represents the minimum inertia.

The second parameters is the free bending length l_0 that depends on the effective length l of the bar and by the kind of constraints. In Figure 5.4 some common situation are pointed out.

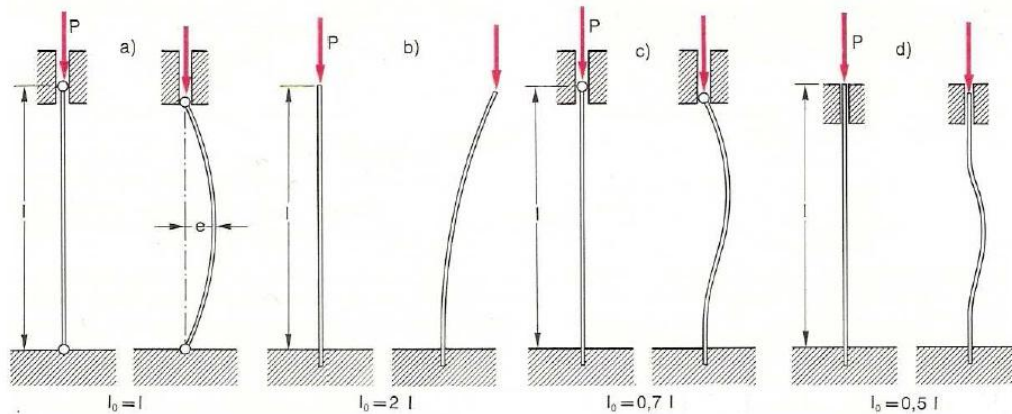


Figure 5.4 Value of l_0 with its dependency on constraints types

And so it is possible to evaluate the slinness parameters defined as:

$$\lambda = \frac{l_0}{i_{min}}$$

If λ is higher must be considered the peak load condition during the design. In other case, the normal compression condition design is still valid.

Eulero theory brings to the definition of a critical load F_{cr} obtained from the equilibrium condition $M_e=M_i$:

$$F_{CR} = \frac{\pi^2 * E * I_{min}}{l_0^2}$$

With a simple mathematical consideration it is possible to obtain:

$$\frac{F_{CR}}{A} = \frac{\pi^2 * E * I_{min}}{l_0^2 * A} = \frac{\pi^2 * E * i_{min}}{l_0^2}$$

And calling $\sigma_{CR} = \frac{F_{CR}}{A}$ the critical strain condition, will be:

$$\sigma_{CR} = \frac{\pi^2 * E}{\lambda}$$

To verify the peak load condition does not occurs must be verified the condition:

$$F \leq \frac{F_{CR}}{N}$$

or:

$$\sigma \leq \frac{\sigma_{CR}}{N}$$

Where N depends on the considered material:

- N=3÷5 for iron/steel;
- N=7÷8 for pig iron;

With dynamic stresses these coefficients must be multiplied by 2÷3.

5.3.2. Peak analysis applied to supports

Problem inputs are:

- External diameter of supports;
- Thickness or internal diameter of supports;
- Acceleration (External load);
- Young modulus of the material (titanium $E=104$ GPa);
- Angles of supports with respect to the base or the angle generated between supports legs themselves;
- Distance between the base and the satellite;

In Figure 5.5 it is showed the situation in which the external load, represented by the force generated by the acceleration imposed ad 600 m/s^2 , acts on instrument base support. The configuration showed is the one in which the angle considered is about 45° and the distance between the instrument base and the satellite is 90 mm.

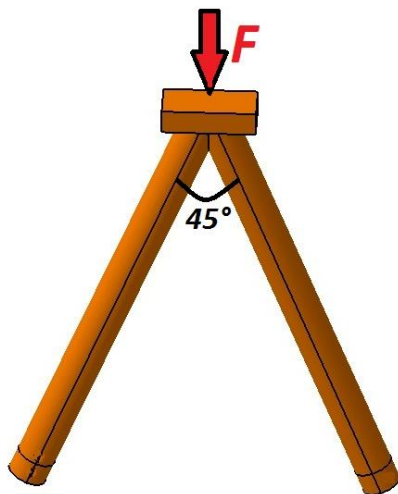


Figure 5.5 External load applied to the instrument support

Imposing the thickness of the pipe at 0.15 mm it have been possible to conduct the peak load analysis for many values of external diameter. An Excel Table have been created in order to manage this problem (please consults the Appendix 1 at the end of the thesis).

Here the analysis is pointed out for these data:

- Acceleration: 600 m/s²;
- Instrument mass: 0.9 kg;
- External diameter: 8.5 mm;
- Thickness: 0.15 mm;
- Distance between satellite and instrument base: 90 mm;
- Material: Titanium E=104 GPa;

Problem solution:

The annulus area is:

$$A = \pi * (R^2 - r^2) = 0.00000393 \text{ m}^2$$

The inertia is given by:

$$I = \frac{\pi}{64} * (D_e^4 - D_i^4) = 3.43 * 10^{-11} \text{ m}^4$$

Applying the formula to find the minimum inertial radius:

$$i_{min} = \sqrt{\frac{I_{min}}{A}}$$

and considering that the length of the supports have been evaluated in relation of supports angles, looking to [Figure 5.4](#) and considering the kind of constraints used for these parts, the value of l_0 have been determined by:

$$l_0 = 0.5 * l = 0.049 \text{ m}$$

with $l = 97$ mm. Is than possible to find the value of the slimmess:

$$\lambda = \frac{l_0}{i_{min}} = 16.49$$

Since it is an higher value, it have been necessary to conduct a peak load evaluation.

Chapter 5

The force that is acting as external load have been found starting from the acceleration:

$$F_{TOT} = m * a = 5230 \text{ N}$$

This force acts on support like in [Figure 5.5](#) and so the force have been resolved into two components, the normal and the tangential one. The value considered is the tangential one that is calculated by means of this formula:

$$F = F_{TOT} * \cos(22.5^\circ) = 4895 \text{ N}$$

Applying the Eulero formula:

$$F_{CR} = \frac{\pi^2 * E * I_{min}}{l_0^2} = 14840 \text{ N}$$

And considering a safety coefficient of $N=3$:

$$F \leq \frac{F_{CR}}{N}$$

$$4895 \text{ N} \leq 4946 \text{ N}$$

That is verified.

Consideration are that this value is the lower limit since, as it is possible to see in the Appendix 1, the situation in which the external diameter is equal to 8.25 mm is not verify. For diameter greater than the 8.5 mm the results are verified.

5.4. Thermal analysis of supports

5.4.1. Thermal analysis theory

Physics describe the thermal conductivity, k , like the property of a material to conduct heat. Thermal conductivity is measured in watts per Kelvin per meter ($\text{W}\cdot\text{K}^{-1}\cdot\text{m}^{-1}$). The reciprocal of thermal conductivity is named thermal resistivity. The thermal problem can be conveniently solved using the electrical analogy; the electrical resistance is given by:

$$R_{el} = \frac{\rho * L}{S}$$

Where ρ indicates the electric conductivity, L the length and S is the section of the conductor. Similarly, the thermal resistance is:

$$R_{TH} = \frac{L}{\lambda * S} = \frac{1}{\lambda} \frac{L}{S}$$

Where λ represents the thermal conductivity, different for all materials, with dimensions [$\text{W}/\text{m}\cdot\text{K}$].

5.4.2. Thermal analysis applied to supports

Results presented in Paragraph 5.2.2, were verified in terms of thermal resistance. In this case, the overall thermal resistance between the satellite frame and the optical bench must be larger than 10^3 K/W. The inputs are:

The input data to this problem are:

- External diameter;
- Internal diameter or wall thickness;
- Distance between the instrument base to the satellite;
- Titanium thermal conductivity = 21,9 W/m*K;

Chapter 5

Also in this case will be considered the external diameter equal to 8.5 mm with a wall thickness equal to 0.15 mm. All value of thermal analysis problem solution are reported into [Appendix 2](#) at the end of this thesis.

Problem solution:

It can be resolved applying the formula for the thermal resistance:

$$R_{TH} = \frac{L}{\lambda \cdot S} = 1130 \text{ K/W}$$

Since its order is greater than 1000 K/W this can be considered as a good result. In case of thermal analysis, values of external diameter from 4 mm to 9.5 mm give verified condition with wall thickness equal to 0.15mm.

5.5. Peak load and thermal analysis comparison

5.1. Peak load and Thermal Analysis comparison (WT=0.15mm)

De	Di	Peak load Analysis	Thermal Analysis
4	3,7	FALSE	TRUE
4,25	3,95	FALSE	TRUE
4,5	4,2	FALSE	TRUE
4,75	4,45	FALSE	TRUE
5	4,7	FALSE	TRUE
5,25	4,95	FALSE	TRUE
5,5	5,2	FALSE	TRUE
5,75	5,45	FALSE	TRUE
6	5,7	FALSE	TRUE
6,25	5,95	FALSE	TRUE
6,5	6,2	FALSE	TRUE
6,75	6,45	FALSE	TRUE
7	6,7	FALSE	TRUE
7,25	6,95	FALSE	TRUE
7,5	7,2	FALSE	TRUE
7,75	7,45	FALSE	TRUE
8	7,7	FALSE	TRUE
8,25	7,95	FALSE	TRUE
8,5	8,2	TRUE	TRUE

8,75	8,45	TRUE	TRUE
9	8,7	TRUE	TRUE
9,25	8,95	TRUE	TRUE
9,5	9,2	TRUE	TRUE
9,75	9,45	TRUE	FALSE
10	9,7	TRUE	FALSE

Table 5.1 shows the results of the two analyses performed to identify the best solution. For instance all values in the range of external diameter between 8.5 to 9.5 verify both analyses in the case of 0.15 mm of wall thickness (WT). By means of this Excel table it have been possible to achieve the minimum condition of wall thickness in which, at least one outer diameter, verify both thermal and peak load analysis [Appendix 1,2]. This occurs with a WT equal to 0.17 mm. Figure 5.6 shows the instrument support with the verified geometry:

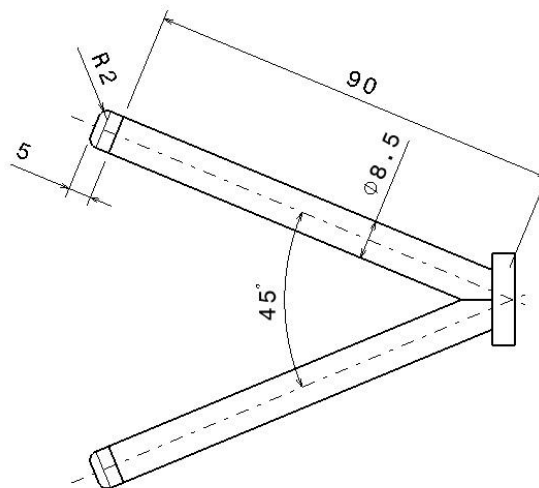


Figure 5.6. *Instrument support dimensions*

Chapter 6

Final Model Design

6.1. Definitive ribbed instrument base

According to the verified condition of peak load and thermal resistance analysis of the base supports, discussed in Chapter 5, the final model, of the base instrument, was modified. In particular, the ribs position and geometry was changed to reach the required natural frequency of the entire model. The considered condition is the one in which the instrument supports have a tubular V-Shape with an angle of 45° between the two legs composing the support.

With this configuration, the best solution for the support the base, that allows reaching the desired natural frequency is shown in [Figure 6.1](#).

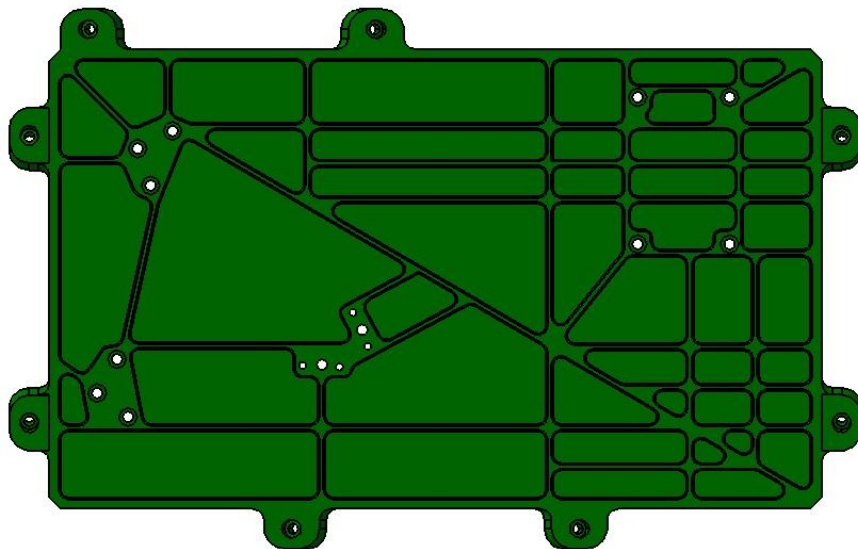


Figure 6.1. *Instrument base support*

In [Figure 6.2](#) is showed the perspective view of the same component.

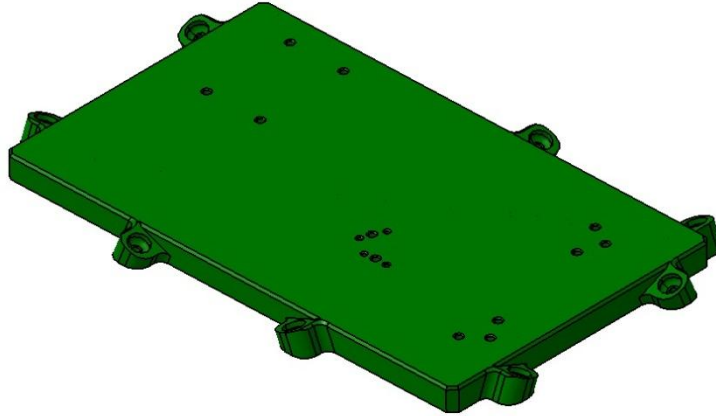


Figure 6.2. *Instrument base support perspective*

This part is realized by an aluminum alloy and gives a low contribution in terms of total mass since it weight is about 0.20 kg. Ribs have been modeled with an height of 10 mm and thickness equal to 2 mm while, the top surface, is a thin layer with height equal to 0.5 mm. [Figure 6.3](#) shows the completed model.

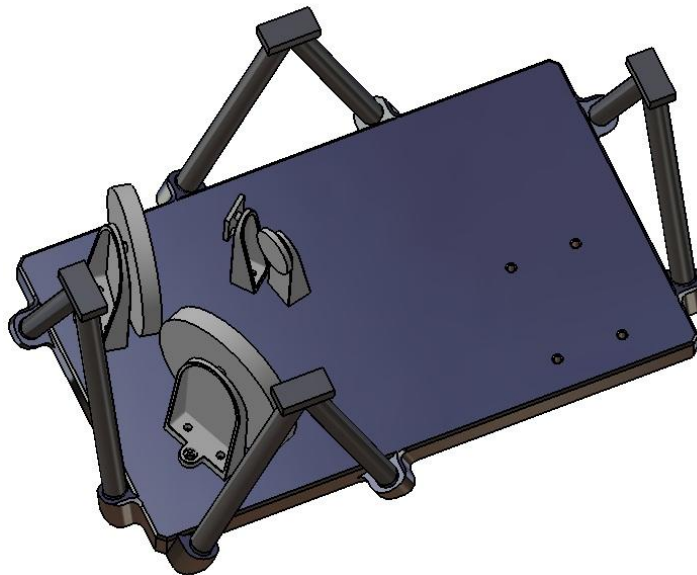


Figure 6.3. *Complete model*

A qualitative 2d draw, showed in [Figure 6.4](#), gives an idea of the main dimensions.

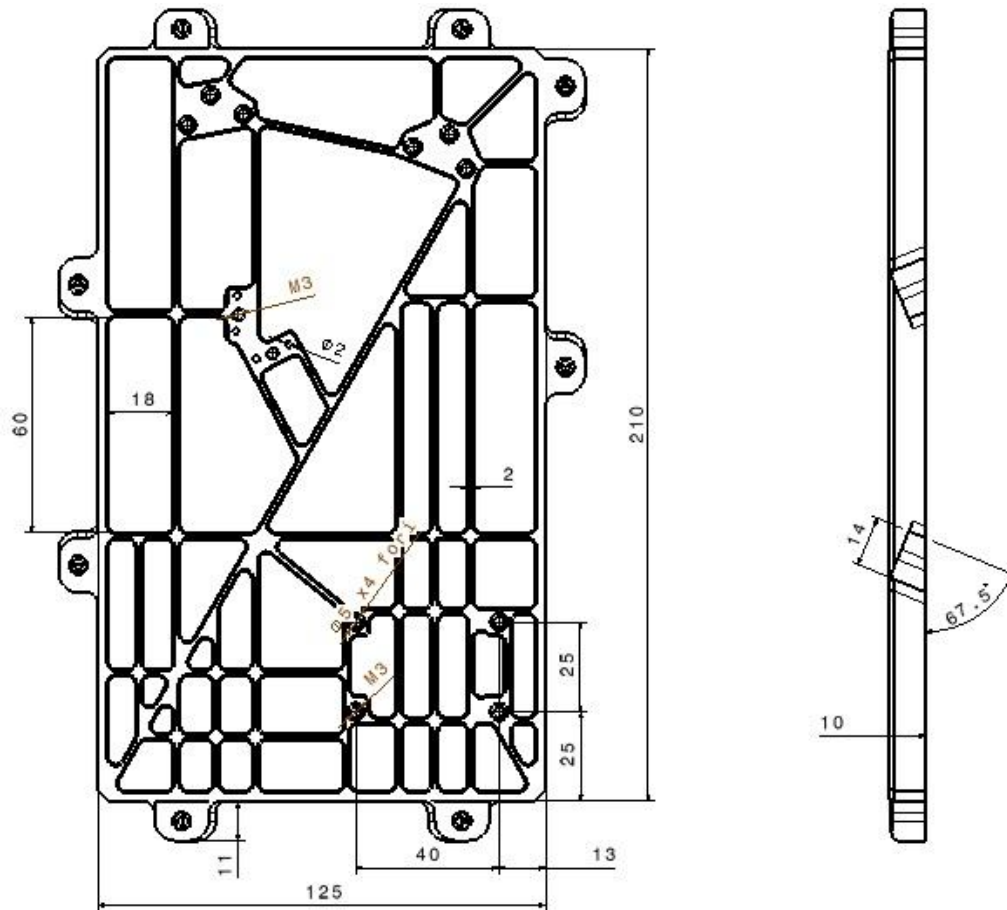


Figure 6.4 2D draw of Instrument base

6.2. Total model analysis

This chapter presents the FEM analyses performed to verify the whole assembly natural frequencies and the resistance to vibrations during the launch. [Figure 6.5](#) shows the total model under investigation for the frequency analysis. As it is possible to see for tubular V-shape parts and, for all the ones that have low thickness, have been adopted the shell elements that permit to approximate the real situation by means of FEM analysis.

Since, the moveable lens and its electric motor are not subject of this thesis work and, since the study that is treating these parts predict their total mass equal to 0.4 kg, a rough box is used to model these parts in order to evaluate the total

Chapter 6

model natural frequency by FEM analysis. Obviously, the value reached in these analysis (frequency and static) could have some changes due to the application of the real electric motor and lens.

Figure 6.5 shows the total model under investigation for the frequency analysis.

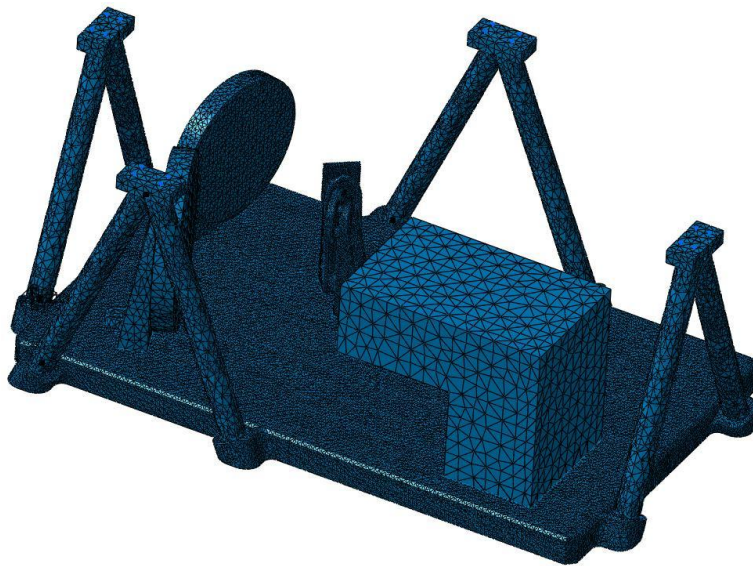


Figure 6.5 *Definitive model frequency analysis*

The value of natural frequency for the definitive model is equal to 163 Hz and at this frequency the model presents a vibration mode that can be associate mainly to the instrument base, as it is showed in Figure 6.6.

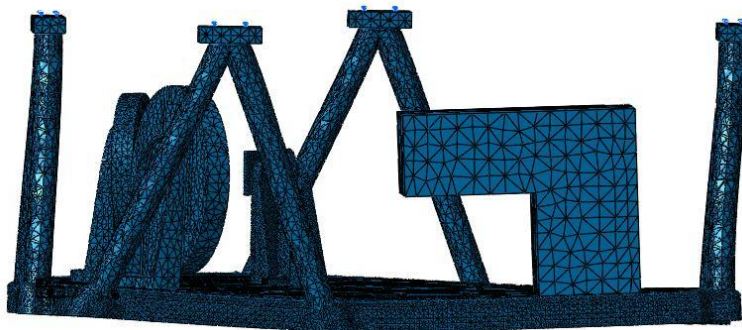


Figure 6.6 *First vibration mode*

Static analysis have been conducted also for this final model considering the acceleration of 600 m/s^2 acting along x and z axis. Figure 6.7 shows the first case in which the acceleration acts along the z-axis and, Figure 6.8 refers to the case of acceleration acting along the x-axis.

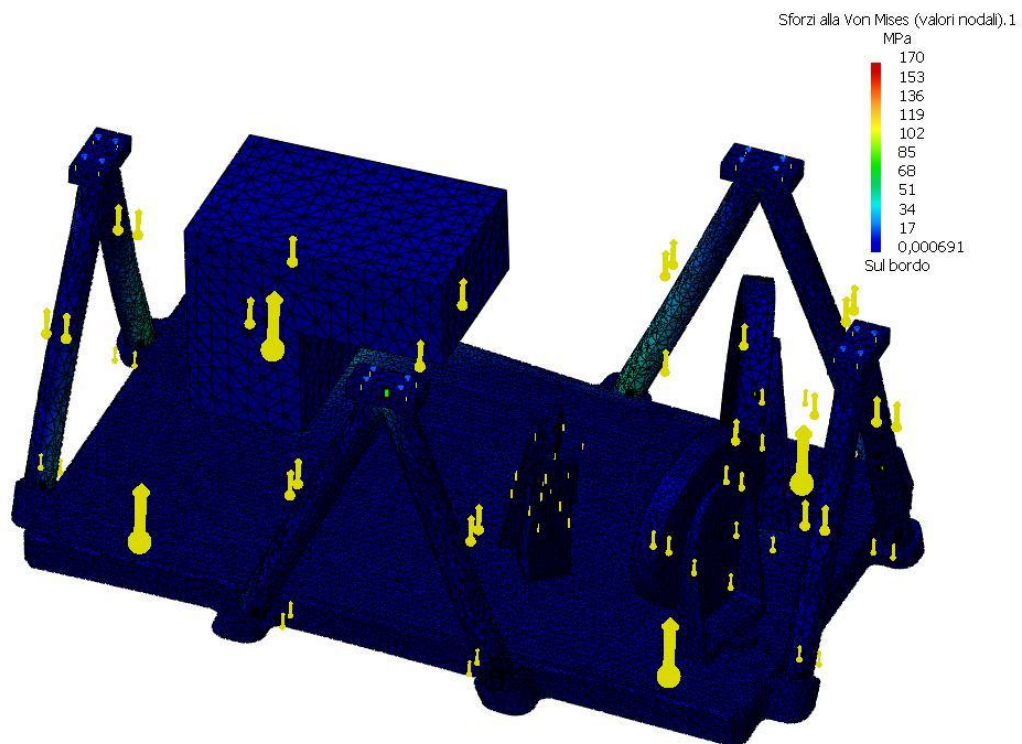


Figure 6.7 *Acceleration acting along z-axis*

The value of stress passes from the minimum at about 0 MPa to the maximum at 170 MPa. This value is reached at contact point between the instrument support and the base. But since they are in the safety range, with a maximum stress value extremely far from the yield point, also this verification can be considered validate.

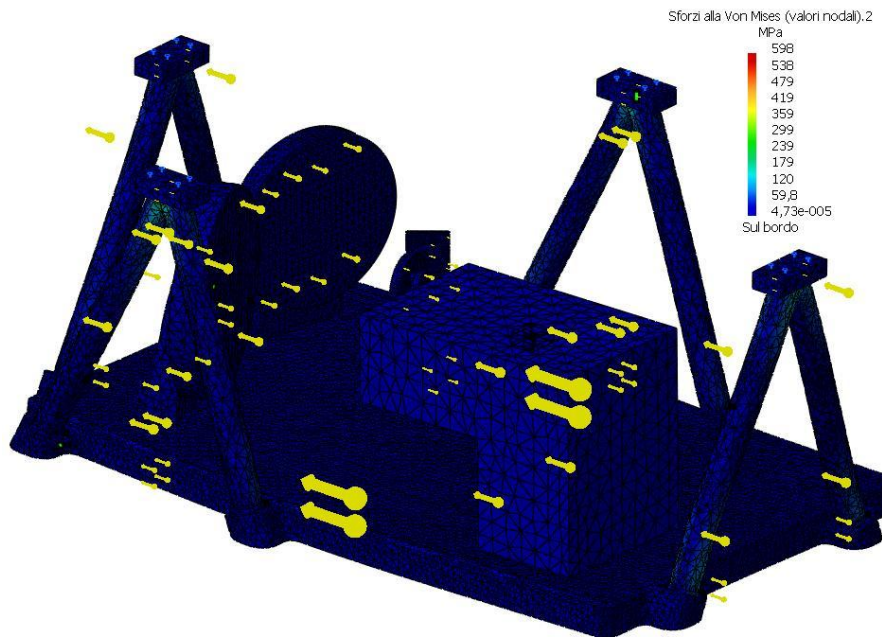


Figure 6.8 Total model analysis with acceleration acting on x-axis

Results of the case in which the acceleration acts along the x-axis presents a peak of value at 590 MPa. But, analyzing carefully results, it is possible to notice that this maximum value is reached in correspondence of the junction point between the two legs of the instrument support. In fact, as it is possible to see in [Figure 6.8](#), the entire model has a stress value at the minimum condition (blue zones) with the maximum value at about 170 MPa.

For these reason the model can be considered well defined also the aspect of the resistance at an imposed acceleration. The eventual peak of the stress can be controlled by a properly definition of the junction point of the supports.

[Table 6.1](#) summarizes principal characteristics of this instrument model.

Table 6.1 Principal characteristics of total model

Mass	1 Kg
First natural frequency	163 Hz
Maximum value of stress under load (acceleration) condition	170 MPa

Chapter 7

TM Covering systems

7.1 Thermal mapper cover

This chapter represents the last part of this thesis work and it deals with the preliminary study of a covering system for the Thermal Mapper. This cover has to insulate the entire instrument and, at the same time, protect it from eventual debris. Looking at previous study, conducted for MIMA space mission [12], it has been decided to maintain similar design considerations; material and geometry are the ones applied to that covering system.

7.1.1. Covering system model

The modeled covering system is showed in [Figure 7.1](#).

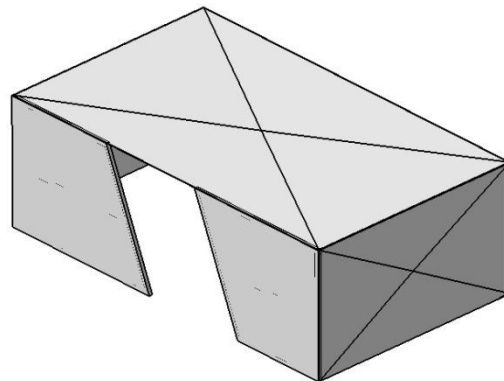


Figure 7.1 *Coverign system*

As it is possible to see, it is composed by a rectangular box with three pyramidal faces, one open side at the bottom and flat planar face with beam entrance at the front.

Pyramidal faces are useful to give at the model high value of stiffness and, so, it is possible to reach high value of natural frequency.

Founding on MIMA study [12], the Thermal Mapper covering system, has been designed considering that, the displacement of the pyramid top greater than 1mm, with respects to its base, does not contribute to enlarge the value of natural frequency. Moreover, the wall thickness have been imposed at the constant value of 0.3 mm. Figure 7.2 shows the top part of the covering system.

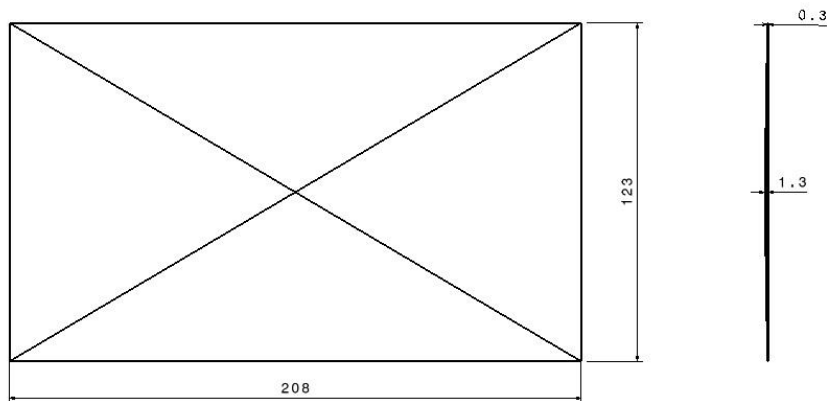


Figure 7.2 Top of the TM covering system. Principal dimensions.

Instead, Figure 7.3 shows the axonometric view of the thermal mapper cover in which it is possible to see the mounting system that will permits, by means of M3 screws, to mount the cover to the optics bench.

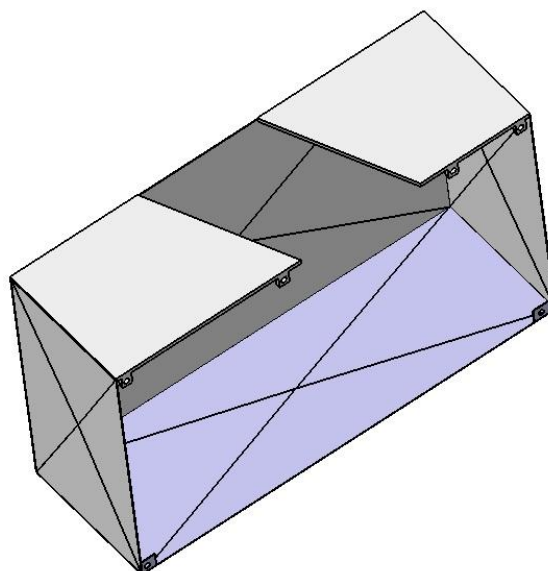


Figure 7.3 Axonometric view of Thermal Mapper Covering system

The frontal part of the cover is done by a ribbed plane surface considering that, the study conducted for MIMA's mission [12], takes into account the presence of ribs into a surface.

Looking the results obtained in this previous study, some considerations are applied to this case and a model have been obtained and it is showed in [Figure 7.4](#).

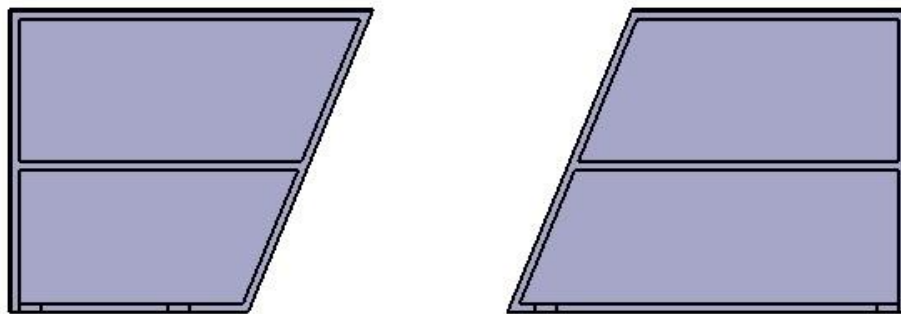


Figure 7.4 *Frontal part of the thermal mapper cover system*

Ribs geometry has rectangular cross section area with height equal to 1.5 mm and width equal to 2 mm. Surface layer has thickness of 0.3 mm.

7.1.2. Frequency analysis on TM's cover system

Considering as material the Composite Fiber ([Table 1.3](#)), FEM analysis have been conducted in order to point out value of natural frequency. Shell elements were adopted since the wall thickness is extremely low (0.3 mm). The total mass of the model is 37 g.

Imposing clamps constraints to the model, it reaches the natural frequency at 185 Hz. [Figure 7.5](#) shows the FEM result.

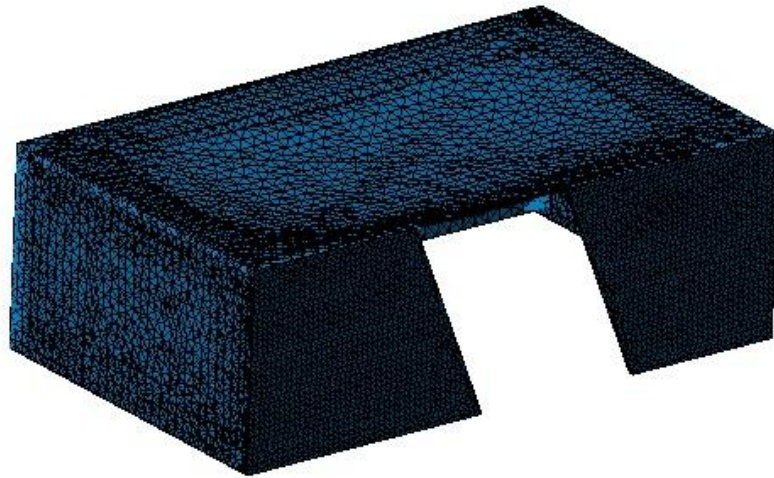


Figure 7.5 FEM analysis at 183 Hz for the cover system

This value of natural frequency can be commented saying that, as well as the results obtained from MIMA covering system, also in this case, the first vibration mode can be associate to the upper face of the box [12]. Figure 7.6 shows this part analyzed imposing clamps constraints, in order to focus the reader attention on, the surface bending motion. Natural frequency of the part is 384 Hz.



Figure 7.6 Lateral view of top box surface at 384 Hz

7.1.3. Static analysis with imposed acceleration on TM's cover system

Figure 7.7 shows the worst condition obtained from the static analysis conducted applying an acceleration of 600 m/s^2 along principal axis directions (x,y,z). The highest value is reached when the acceleration acts along the z-axis and the value of stress is 44 MPa.

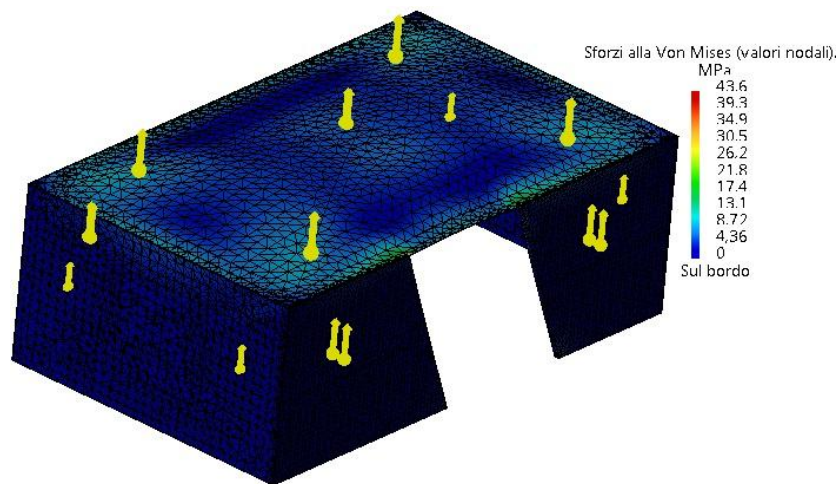


Figure 7.7 Static analysis with acceleration acting along z-axis

7.2. Thermal Mapper covering system conclusion

With its extremely low mass at 37 g and its high natural frequency of 185 Hz, the model of covering system for the thermal mapper, here studied, represent the best solution for this preliminary study. Coming out from the same considerations done for the MIMA mission [12] this model can be studied in the future by considering a new mounting system that will permits to join this parts with the optics bench.

Chapter 8

Conclusions

Born from the collaboration between American and European space agencies, the EJSM project (acronym for Europa Jupiter System Mission) will employ two spacecrafts for the Jupiter's system exploration. Especially, ESA has the hard work to build two modules: Jupiter Ganymede Orbiter (JGO) and Jupiter Europa Orbiter (JEO). The mission's reference date is 2020, year in which the two spacecrafts will be launched by means of Ariane V. The satellites will take six years to reach the final Jupiter's orbit and during three years it will be able to send to Earth information about the planet.

This thesis concerned the preliminary mechanical design of the Thermal Mapper (TM) that will be onboard the JGO module. This instrument will be mainly composed by a structure upon which five optics are mounted with their supports, conveniently oriented, and its task will consist in describing Jupiter's atmosphere characteristics, furthermore determining the volcanic activities of Io and Icy satellites.

The initial stages of the thesis's work consisted in the establishment of the minimum allowable dimension of the optics bench. A first assessment was conducted obtaining dimensions for the rectangular base, of the bench, of 170 mm x 120 mm.

Starting from these initial parameters, an additional study was performed in order to properly define the support base; for this, four cases were analyzed: the single plane, the double plane, the single ribbed plane and the double ribbed plane. FEM analysis pointed out that the best solution, in terms of natural frequency and mass, is given by the single ribbed plane.

The second stage of the thesis's work was to define the optics supports with a higher level of detail. Optics were divided in two categories (large/heavy and small/light optics), it was possible to define two different kinds of supports, one

Chapter 8

for each category, by taking in consideration the disposition and orientation of the lenses. The best solution for both types of supports were found through the use of FEM analysis. The fifth lens which is part of a scanning mechanism, was not taken into account since it is study of a dedicated work and here is treated as a rectangular box with equivalent mass of 0.4 kg.

Considering these new optics supports an intermediate evaluation of the bench was conducted. Considering clamps and hinges constraints, instead the real constraint given by the bench supports, ribs disposition and geometry were evaluated. This pointed out new dimension for it. 210 mm x 125 mm x 6 mm, 0.139 kg and 252 Hz are the best significant characteristics found for this intermediate model.

Afterwards, the design of the instrument's supports was executed, in terms of thermal load and peak load assessment. Such supports were designed to be tubular truss, made from a Titanium alloy. The studies were done considering different angles forming the V-shape and taking into account that these parts will be not only supports, but will also have the task of reducing the conductive heat exchange between the instrument base and the satellite.

After the thermal load and peak load assessments, solutions were selected identifying a range of external and internal diameters for which both analyses were verified. The solutions were found in correspondence of an outer diameter equal to 8.5 mm and a wall thickness of about 0.15 mm while the V angle was imposed at 45°.

Then, with the design of the instrument supporting structure defined, it was possible to perform a more detailed analysis of the optics bench.

The last part of the thesis deals with the definition of the covering system for the thermal mapper. The proposed solution comes from a previous study of an instrument for space application. In fact, the new covering model, for the JGO mission, was obtained with the same design consideration derived for the MIMA spectrometer.

Assembling all components together, a total model was obtained. Total mass of the Thermal Mapper structure is 0,8 kg with natural frequency at 160 Hz that

are compatible with the instrument requirements of total mass 5 kg, min natural frequency above 140 Hz.

It is relevant to note, that the work developed along this pages represent only the starting point for future studies that should involve a more detailed design of the components. In particular, future studies should be done on the instrument base optimizing ribs geometry. Furthermore, since in this thesis it is not considered the definitive model of the scanning mirror with its motor, future studies will need to consider to the final system to guarantee that mass budget and natural frequency would be always verified. The starting point of the study should be the evaluation of different kind of instrument supports in terms of material and geometry. In other case, it would be advisable to consider another value of outer diameter for the V-shaped tubular support considered in this thesis (8.5 mm).

Chapter 9

References

- [1] ESA www.esa.int
- [2] NASA www.nasa.gov
- [4] Z.Hasin, “the elastic moduli of heterogeneous materials”, J.Appl.Mech. 29,1962, pp- 143-150
- [5] Z.Hasin, B.W.Rosen, “the elastic moduli of fiber-reinforced materials”, J.Appl.Mech 31, 1964,pp 223-505
- [6] B.Budiansky, “On the elastic moduli of heterogeneous material”, JMPS 13, 1965, pp.223-227
- [7] European Cooperation ECSS for space standardization, “ECSS-E-30 Part 2A- Structural”, 25 April 2000
- [8] A.Wielders, “Payload definition document for the Jupiter Ganymede Orbiter of the Europa Jupiter System mission”, EJSM JSTD, ESA study team 27 March 2009
- [9] E. Perez, “Arianne V. User’s manual”, July 2008
- [10] A.Boutonnet, J.Schoenmaekers, P.de Pascale, E.Canalias, “LAPLACE: Mission Analysis Guidelines”, 14 November 2008
- [11] L.Baldassini, “Vademecum per disegnatori e tecnici”, Hoepli Editore, 1998, 12esima edizione
- [12] J.Pucciani, M.Vismara, “Progettazione e verifica di una struttura di protezione termica e dalla contaminazione nell’atmosfera di Marte”, 2008-2009

Chapter 10

Appendix

1)

De	Di	Arca	Inerzia I	Raggio di inerzia minimo imin	L0	Snellezza λ	E GPa	N	Fcr	FsFcr/N
0,004	0,00366	0,00000205	3,75803E-12	0,001355443	0,048707649	35,934863	104	3	1625,918092	FALSO
0,00425	0,00391	0,00000218	4,54195E-12	0,001443749	0,048707649	33,736912			1965,085156	FALSO
0,0045	0,00416	0,00000231	5,42802E-12	0,001532066	0,048707649	31,792143			2348,443745	FALSO
0,00475	0,00441	0,00000245	6,42249E-12	0,00162039	0,048707649	30,059221			2778,701673	FALSO
0,005	0,00466	0,00000258	7,53161E-12	0,00170872	0,048707649	28,505338			3258,566754	FALSO
0,00525	0,00491	0,00000271	8,76165E-12	0,001797057	0,048707649	27,104126			3790,746802	FALSO
0,0055	0,00516	0,00000285	1,01189E-11	0,001885398	0,048707649	25,834149			4377,949631	FALSO
0,00575	0,00541	0,00000298	1,16095E-11	0,001973743	0,048707649	24,677804			5022,883055	FALSO
0,006	0,00566	0,00000311	1,32399E-11	0,002062092	0,048707649	23,620498			5728,254887	FALSO
0,00625	0,00591	0,00000325	1,50162E-11	0,002150445	0,048707649	22,650035			6496,772943	FALSO
0,0065	0,00616	0,00000338	1,69447E-11	0,0022388	0,048707649	21,756142			7331,145035	FALSO
0,00675	0,00641	0,00000351	1,90316E-11	0,002327158	0,048707649	20,930103			8234,078978	FALSO
0,007	0,00666	0,00000365	2,12833E-11	0,002415518	0,048707649	20,164477			9208,282587	FALSO
0,00725	0,00691	0,00000378	2,3706E-11	0,002503879	0,048707649	19,452873			10256,46367	FALSO
0,0075	0,00716	0,00000391	2,6306E-11	0,002592243	0,048707649	18,789768			11381,33005	FALSO
0,00775	0,00741	0,00000405	2,90894E-11	0,002680609	0,048707649	18,170370			12585,58954	FALSO
0,008	0,00766	0,00000418	3,20626E-11	0,002768975	0,048707649	17,590495			13871,94995	FALSO
0,00825	0,00791	0,00000432	3,52318E-11	0,002857344	0,048707649	17,046479			15243,11909	VERO
0,0085	0,00816	0,00000445	3,86033E-11	0,002945713	0,048707649	16,535097			16701,80479	VERO
0,00875	0,00841	0,00000458	4,21834E-11	0,003034083	0,048707649	16,053497			18250,71484	VERO
0,009	0,00866	0,00000472	4,59782E-11	0,003122455	0,048707649	15,599152			19892,55708	VERO
0,00925	0,00891	0,00000485	4,99941E-11	0,003210827	0,048707649	15,169812			21630,0393	VERO
0,0095	0,00916	0,00000498	5,42373E-11	0,003299201	0,048707649	14,763470			23465,86933	VERO
0,00975	0,00941	0,00000512	5,87141E-11	0,003387575	0,048707649	14,378325			25402,75498	VERO
0,01	0,00966	0,00000525	6,34307E-11	0,00347595	0,048707649	14,012761			27443,40406	VERO

De	Spessore	Di	Sezione	Angolo	Angolo 2	Dist Sat-Base	Lunghezza	Conducibilità Termica	Resistenza termica	
4	0,34	3,66	0,00000205	67,5	22,5	90	0,097415298	21,9	2174,630529	VERO
4,25		3,91	0,00000218	1,17809725	0,39268908				2041,381109	VERO
4,5		4,16	0,00000231						1923,518459	VERO
4,75		4,41	0,00000245						1818,522909	VERO
5		4,66	0,00000258						1724,396465	VERO
5,25		4,91	0,00000271						1639,534434	VERO
5,5		5,16	0,00000285						1562,633194	VERO
5,75		5,41	0,00000298						1492,622746	VERO
6		5,66	0,00000311						1428,616625	VERO
6,25		5,91	0,00000325						1369,874165	VERO
6,5		6,16	0,00000338						1315,77171	VERO
6,75		6,41	0,00000351						1265,780384	VERO
7		6,66	0,00000365						1219,448745	VERO
7,25		6,91	0,00000378						1176,389114	VERO
7,5		7,16	0,00000391						1136,266702	VERO
7,75		7,41	0,00000405						1098,790887	VERO
8		7,66	0,00000418						1063,708164	VERO
8,25		7,91	0,00000432						1030,796402	VERO
8,5		8,16	0,00000445						999,8601351	FALSO
8,75		8,41	0,00000458						970,7266813	FALSO
9		8,66	0,00000472						943,2429134	FALSO
9,25		8,91	0,00000485						917,2725689	FALSO
9,5		9,16	0,00000498						892,6839899	FALSO
9,75		9,41	0,00000512						869,3982177	FALSO
10		9,66	0,00000525						847,287378	FALSO

2)